



**HAL**  
open science

## Corneal stromal stem cells restore transparency after N 2 injury in mice

Djida Ghoubay, Marie Borderie, Kate Grieve, Raphaël Martos, Romain Bocheux, Thu-Mai Nguyen, Patrice Callard, Alain Chédotal, Vincent M. Borderie

► **To cite this version:**

Djida Ghoubay, Marie Borderie, Kate Grieve, Raphaël Martos, Romain Bocheux, et al.. Corneal stromal stem cells restore transparency after N 2 injury in mice. *Stem Cells Translational Medicine*, 2020, 10.1002/sctm.19-0306 . hal-02586732

**HAL Id: hal-02586732**



<https://hal.sorbonne-universite.fr/hal-02586732v1>

Submitted on 15 May 2020

**HAL** is a multi-disciplinary open access archive for the deposit and dissemination of scientific research documents, whether they are published or not. The documents may come from teaching and research institutions in France or abroad, or from public or private research centers.

L'archive ouverte pluridisciplinaire **HAL**, est destinée au dépôt et à la diffusion de documents scientifiques de niveau recherche, publiés ou non, émanant des établissements d'enseignement et de recherche français ou étrangers, des laboratoires publics ou privés.

# Corneal stromal stem cells restore transparency after N<sub>2</sub> injury in mice

Djida Ghoubay<sup>1,2</sup>  | Marie Borderie<sup>2</sup> | Kate Grieve<sup>1</sup> | Raphaël Martos<sup>3</sup> | Romain Bocheux<sup>4</sup> | Thu-Mai Nguyen<sup>5</sup> | Patrice Callard<sup>6</sup> | Alain Chédotal<sup>1</sup> | Vincent M. Borderie<sup>1,2</sup> 

<sup>1</sup>Institut de la Vision, Sorbonne Université, INSERM, CNRS, Paris, France

<sup>2</sup>Centre Hospitalier National d'Ophthalmologie des 15-20, DHU Sight Restore, INSERM-DHOS CIC, Paris, France

<sup>3</sup>Laboratoire de Recherche Vasculaire Translationnelle, INSERM U1148, Université Paris Diderot, Sorbonne Paris Cité, Paris, France

<sup>4</sup>Laboratoire d'Optique et Biosciences (LOB) École polytechnique, CNRS UMR 7645, INSERM U 1182, Palaiseau cedex, France

<sup>5</sup>Institut Langevin Ondes et images CNRS UMR 7587, INSERM U979 Physiques des ondes pour la médecine, ESPCI, Paris, France

<sup>6</sup>Sorbonne Université, AHP, Hôpital Pitié Salpêtrière, Paris, France

## Correspondence

Vincent M. Borderie, MD, PhD, Institut de la Vision, Sorbonne Université, INSERM, CNRS, 17, Rue Moreau, Paris 75012, France.  
Email: vincent.borderie@upmc.fr

## Funding information

European Research Council SYNERGY, Grant/Award Number: 610110; "Fondation pour la Recherche Médicale", Grant/Award Number: DCM2012122579

## Abstract

Corneal scarring associated with various corneal conditions is a leading cause of blindness worldwide. The present study aimed to test the hypothesis that corneal stromal stem cells have a therapeutic effect and are able to restore the extracellular matrix organization and corneal transparency in vivo. We first developed a mouse model of corneal stromal scar induced by liquid nitrogen (N<sub>2</sub>) application. We then reversed stromal scarring by injecting mouse or human corneal stromal stem cells in injured cornea. To characterize the mouse model developed in this study and the therapeutic effect of corneal stromal stem cells, we used a combination of in vivo (slit lamp, optical coherence tomography, in vivo confocal microscopy, optical coherence tomography shear wave elastography, and optokinetic tracking response) and ex vivo (full field optical coherence microscopy, flow cytometry, transmission electron microscopy, and histology) techniques. The mouse model obtained features early inflammation, keratocyte apoptosis, keratocyte transformation into myofibroblasts, collagen type III synthesis, impaired stromal ultrastructure, corneal stromal haze formation, increased corneal rigidity, and impaired visual acuity. Injection of stromal stem cells in N<sub>2</sub>-injured cornea resulted in improved corneal transparency associated with corneal stromal stem cell migration and growth in the recipient stroma, absence of inflammatory response, recipient corneal epithelial cell growth, decreased collagen type III stromal content, restored stromal ultrastructure, decreased stromal haze, decreased corneal rigidity, and improved vision. Our study demonstrates the ability of corneal stromal stem cells to promote regeneration of transparent stromal tissue after corneal scarring induced by liquid nitrogen.

## KEYWORDS

cell therapy, corneal stromal scar, limbal stromal stem cells, sphere formation

## 1 | INTRODUCTION

The cornea is the outermost layer of the eye and it forms the central part of the ocular surface. It provides two thirds of the optical power of the eye, and refracts and focuses incident light on retina. The cornea plays a protective role in the eye by acting as an external barrier to infectious agents.<sup>1</sup> It is composed of three tissue layers derived from two embryonic germ tissues: a stratified corneal epithelium of surface ectoderm origin, a stromal layer populated by keratocytes and composed of highly aligned collagen fibrils, and a monolayer of endothelial cells covering the posterior corneal surface.<sup>2-4</sup> The latter two layers derive from the neural crests.<sup>5-8</sup>

The stroma constitutes 90% of the corneal thickness and is composed of collagenous lamellae consisting of tightly packed collagen fibrils embedded in a hydrated matrix of glycoproteins and proteoglycans. The parallel arrangement and the uniform spacing of the collagen fibrils are thought to result in destructive interference of incoming light rays, thereby reducing scatter and promoting corneal transparency.<sup>9</sup> The keratocytes are a population of mesenchymal neural crest-derived cells,<sup>10</sup> sandwiched between the lamellae, responsible for secretion of the stromal extracellular matrix (ECM), including collagen fibrils and proteoglycans. Mesenchymal neural crest-derived cells are a population of cells with the ability to self-renew and highly multipotent giving rise to peripheral neurons and glia, melanocytes, chondrocytes, osteocytes, and fat cells.<sup>11,12</sup>

Upon injury induced by inflammation or infection, keratocytes are stimulated to either undergo apoptosis<sup>13</sup> or to differentiate toward repair or activated phenotypes characterized by increased cell size with myofibroblast shape and expression of alpha-smooth muscle actin ( $\alpha$ -SMA). These myofibroblasts are responsible for wound contraction as well as for ECM deposition, including opaque collagen type III, and organization during wound repair. Other changes are observed such as an increase in the secretion of the matrix metalloproteinases and collagenases which are responsible for ECM remodeling.<sup>14</sup> Together, these changes occur in the corneal stroma after deep injury and they lead to scarring and loss of corneal transparency.

Corneal allografts remain the gold standard to treat non-inflammatory diseases which lead to a loss of vision. However, the imbalance between donor supply and patient demand poses a public health issue and tremendous efforts are currently being made to develop different strategies to overcome it. Cell therapy using corneal stromal stem cells (SSCs) is one of the new therapeutic approaches that would be of interest to replace conventional donor tissues.

The Funderburgh group at the University of Pittsburgh first characterized the corneal SSCs as a rare population in the human peripheral corneal stroma.<sup>15</sup> SSCs have the potency of multilineage differentiation.<sup>15,16</sup> They have been used in various applications related to ocular regeneration, such as prevention and reduction of corneal scarring<sup>17,18</sup> and generation of corneal tissues mimicking the structure of the human cornea.<sup>19-23</sup> Conversely, corneal fibroblasts, unlike SSC, do not have regenerative effects. They rather induce fibrotic and inflammatory response in vivo.<sup>18,24</sup> SSC can be easily obtained from biopsies taken from the corneal limbus.<sup>16,25</sup> Because

### Significance statement

Corneal scarring is a result of many corneal disorders, including infections, trauma, and genetic diseases, and one of the leading causes of blindness worldwide. Corneal stromal stem cells can be easily retrieved and cultured from patient or donor eyes. They can potentially regenerate the corneal stromal extracellular matrix, which is essential for maintaining corneal transparency. Results of this study demonstrated the therapeutic effect of these adult stem cells in a mouse model of corneal opacification.

these cells are natural progenitors of corneal keratocytes, derived from neural crests, they are expected to provide therapeutic benefit in corneal regeneration based on cell therapy technology.

The present study aimed to test the hypothesis that SSCs have a therapeutic effect and are able to restore the ECM organization and corneal transparency in vivo. Our objective was to monitor engrafted SSC and follow cell and tissue behavior after transplantation, including direct and paracrine stem cell effects as well as changes in tissue structure and physiological properties. We developed a new mouse model of corneal stromal scar induced by liquid nitrogen ( $N_2$ ) application. This mouse model aimed to reproduce changes in corneal shape and structure that disrupt the complex organization of the corneal stroma and cause scarring and opacities. Corneal scarring leading to opacities is the result of many corneal diseases and injuries such as trauma, ocular burn, infectious keratitis, corneal ectatic disorders including keratoconus, genetic corneal disorders including aniridia, and complicated refractive surgery (mainly photorefractive keratectomy [PRK]) for correction of refractive errors (ie, myopia, hyperopia, astigmatism, and presbyopia).<sup>26,27</sup> To characterize the animal mouse model developed in this study and the therapeutic effect of SSC, we used a combination of in vivo (slit lamp, optical coherence tomography [OCT], in vivo confocal microscopy [IVCM], OCT shear wave elastography [OCT-SWE], and optokinetic tracking response [OTR]) and ex vivo (full field optical coherence microscopy [FFOCM], flow cytometry, and histology) techniques.

## 2 | MATERIALS AND METHODS

### 2.1 | Study design and ethics

The purpose of our study was to test the hypothesis that corneal SSCs have a therapeutic effect and are able to restore the ECM organization and corneal transparency in vivo. To test this hypothesis, we developed a mouse model of corneal opacity induced by application of liquid nitrogen ( $N_2$ ) on the corneal surface after epithelial debridement. Corneal opacity, ECM organization, stromal cell density, corneal thickness, corneal rigidity, and fibrotic tissue synthesis were assessed before and after injury with  $N_2$ . Human SSC (HSSC) and murine SSC

(MSSC) were isolated and cultured as previously described.<sup>16</sup> HSSC and MSSC were injected in the mouse corneal stroma. Presence, proliferation, and migration of injected cells in the cornea were assessed by immunostaining and confocal microscopy. The therapeutic effect of SSC was determined by the assessment of corneal opacity, ECM organization and synthesis, stromal cell density, corneal thickness, and corneal rigidity. Imaging techniques used in this study were slit-lamp examination, OCT, IVCM, OCT-SWE, FFOCM, immunofluorescence, and confocal microscopy.

This study was carried out according to the tenets of the Declaration of Helsinki, and it followed international ethic requirements for human tissues. It was submitted to the Ethics Committee of the French Society of Ophthalmology (IRB 00008855 Société Française d'Ophtalmologie IRB#1) who waived approval for this type of study. Donor tissue procurement fulfilled all the legal requirements including absence of donor opposition to donation recorded in the French National Registry of Opposition and positive family testimony. None of the transplant donors were from a vulnerable population and all donors or next of kin provided written informed consent that was freely given.

All experimental procedures were reviewed and approved by Institutional Animal Care and Use Committees (authorization number 4296-2016022516537431).

## 2.2 | Liquid nitrogen-induced corneal injury

Forty-four 4-week-old C57BL/6 mice (Janvier Lab, Le Genest Saint Isle, France) were used in these experiments. Mice were anesthetized by isoflurin 1000 mg/g (Axience, Pantin, France). For topical anesthesia, one drop of oxybuprocaine 1.6 mg/0.4 mL (Théa, Clermont-Ferrand, France) was instilled in the left eye before epithelial debridement. Corneal epithelial debridement was performed with a scalpel (NM medical, Asnières sur Seine, France). Once the epithelium was removed, N<sub>2</sub> was applied with a Q-tip (NM medical) on the corneal surface for 5 seconds in order to disturb the anterior stromal tissue. Briefly, the Q-tip was immersed in liquid nitrogen (−196°C) for 5 seconds, then kept at room temperature (RT; 20°C) for another 5 seconds and applied with no pressure on the corneal surface for 5 seconds. Corneal surface temperature was measured with Ebro thermometer TFN 520 TC Type K (Xylem Analytics, Nanterre, France) in five animals (Figure S1D). The minimal temperature measured in mice eye was obtained 5 seconds following Q-tip application. This figure was −53°C in average. Following removal of the tip, the animal eyelids were closed in order to cover the cornea with the tear film and to quickly recover a normal corneal temperature. Neither saline solution nor other eye drops were applied on the ocular surface. The cornea was not indented by the Q-tip and only the central cornea was in contact with the tip. Ten seconds after removal of the Q-tip, the corneal surface temperature was higher than 0°C (Figure S1E).

In vivo and ex vivo imaging was performed in order to fully characterize the injury induced by N<sub>2</sub>. Mice were observed until the development of corneal opacity. In this experiment, only the left eye was

N<sub>2</sub>-injured, whereas the right eye was used as control. Animals were observed daily after N<sub>2</sub> injury. We did not use any topical or general treatment. The general evaluation criteria were the following: presence of nest, absence of locomotion, bristly and/or dull coat, avoidance behavior, prostration or arched back, tumor, suspicious bleeding, and inflammation. When one of these criteria was observed the animal was sacrificed.

## 2.3 | In vivo imaging

### 2.3.1 | Slit-lamp examination

We performed slit-lamp examination of the anterior segment of the eye, including eyelids, conjunctiva, iris, lens, and cornea. Binocular slit-lamp examination provides a stereoscopic magnified detailed view of the eye structures. In addition, corneas were stained with 0.5%-fluorescein eye-drops (SERB, Paris, France) to detect the presence or the absence of ulceration. Corneas of 26 mice were photographed with a white light illumination. After instillation of one drop of fluorescein, corneas were photographed with a blue cobalt light illumination. Mice were observed before, and 1 day, 1 week, 2 weeks, and 3 weeks after N<sub>2</sub> application. Corneal opacity was scored based on slit-lamp examination before and 3 weeks after N<sub>2</sub> application as follows: 0, transparent cornea; 1, mild corneal haze (sparse or diffuse opacities with clearly visible iris details); 2, severe opacity (translucent opacities obscuring iris details); and 3, severe corneal opacity with no iris visibility.

### 2.3.2 | IVCM and OCT

Corneas of 26 mice were assessed in vivo before and after N<sub>2</sub> injury with IVCM (Heidelberg Retina Tomograph III; Heidelberg Engineering GmbH, Heidelberg, Germany) and spectral-domain OCT (RTVue-100, Optovue Inc, Fremont, California). Quantitative analysis of corneal backscattering corresponding to the hyperreflectivity of the cornea was assessed by ImageJ software (NIH, Madison, Wisconsin) by determining the plot profile of each cross section obtained by OCT.

Mice were anesthetized and high-viscosity eye gel was instilled for IVCM imaging. Series of “en face” images of the entire cornea from the epithelium to the endothelium moving through the depth of the cornea were obtained. The acquired images featured a 400 × 400 μm field of view with a 1 μm lateral resolution. From the images, the following variables were determined: epithelial cell morphology, nuclear and cellular borders and reflectivity, presence of fibrosis and superficial neovascularization, nuclear condensation, keratocyte reflectivity, stromal striae, and endothelial cell morphology. To assess stromal cell density, we considered all en face stromal images obtained by IVCM. When two or more images were taken at the same depth, the image with the highest contrast was selected. Contrast and brightness were enhanced, and cell nuclei were manually counted using the “cell counter” function of the ImageJ software. Only bright and clear oval features were considered to be nuclei.<sup>28</sup>



### 2.3.3 | Optical coherence tomography shear wave elastography

OCT-SWE was performed *in vivo* using a custom-developed setup that has been described previously.<sup>29</sup> Three weeks after N<sub>2</sub> injury, eight mice were anesthetized by intraperitoneal (IP) injection of ketamine (50 mg/kg) and xylazine (5 mg/kg). Controlled shear waves were induced within corneas by a piezoelectric actuator placed at the eye surface and tracked using phase-sensitive spectral-domain OCT. This technology allows corneal biomechanics to be assessed quantitatively as the shear wave velocity increases with corneal rigidity.

### 2.3.4 | Optokinetic tracking response

A virtual-reality system (OptoMotry) was used to assess the visuomotor behavior by quantifying the visual acuity of each eye. Twelve mice were used to assess this experiment. Animals were first habituated in the optokinetic testing device before experiments. The mouse stands on an elevated platform in the epicenter of an arena surrounded by computer monitors, and a camera images the behavior of the animal from above. A cylinder comprised of a sine wave grating is drawn in 3D coordinate space and rotates around the animal. Mice track the grating with reflexive head and neck movements.

The optokinetic response was measured starting with a low spatial frequency sine wave grating at 0.03 cycles/degree with a constant rotation speed of 0.12°/s and 100% contrast. Clockwise and anti-clockwise rotations were presented in random orders to examine the visuomotor function of the left and right eyes, respectively. The spatial frequency of the grating was incrementally increased until the animals failed to respond. The visual acuity was identified as the highest spatial frequency that the mice could track.

### 2.3.5 | Ex vivo imaging

After sacrificing the mouse by CO<sub>2</sub> inhalation, the eyeballs were enucleated and fixed for 16 hours in Davidson's fixative.

### 2.3.6 | Full field optical coherence microscopy

The FFOCM instrument (LLTech, Paris, France) used in this study has been described previously.<sup>30-32</sup> Penetration depth depends on tissue content and transparency. Three weeks after N<sub>2</sub> injury, 14 normal and 14 N<sub>2</sub>-injured corneas were observed. The acquired images consist of 1024 × 1024 pixels over a 780 × 780 μm en face field of view with a 1.6-μm lateral × 1.0 μm axial resolution. One image corresponds to a 1.0-μm-thick corneal section. Images were taken every 1 μm depth step in the central zone of cornea. Three-dimensional image stacks were examined in en face and cross-sectional views using the multiplanar reconstruction software provided with the system.

FFOCM corneal cross sections were used to assess epithelial, stromal, and corneal thicknesses. Thicknesses were measured manually with the ImageJ software at five equally spaced points across the cross section, and the mean values were recorded.

### 2.3.7 | Flow cytometry analysis

The inflammatory response in the mouse model was studied 4, 24, 48, and 72 hours after N<sub>2</sub> injury of the left eye of 4-week-old C57BL/6 mice. A series of 16 mice (3 for each postinjury time point plus 4 controls) was used in this experiment. N<sub>2</sub> was applied to the left eye of each mouse for 5 seconds whereas the right eye served as control. An additional mouse which had not undergone the N<sub>2</sub> process was used at each time point, in order to determine the basal level of inflammation. After each period post N<sub>2</sub> injury, the mice were observed with IVCM. They were then sacrificed and the corneas were retrieved and dissociated using liberase-thermolysine (LTM Roche) 100 μg/mL for 4 hours at 37°C. Cells were washed once and resuspended in 300 μL of PBS buffer for analysis. Background fluorescence and nonspecific binding were measured using unstained cells and isotypic control. Anti-CD11b labeling was performed to observe the inflammatory response rate in flow cytometry. To evaluate cell viability, dissociated cells were resuspended in buffer (1 × 10<sup>6</sup> cells/mL). Propidium iodide (ThermoFisher Scientific, Illkirch, France) was added to the cells at a final concentration of 1 μg/mL and cells were incubated for 30 minutes at 4°C in the dark. Analysis was performed with a FC500 flow cytometer (Beckman Coulter). Flow cytometry files were analyzed using the FlowJo software (Treestar).

### 2.3.8 | EdU injection

Twenty-four hours after N<sub>2</sub> application on mouse cornea, a solution of 5 mg/mL EdU was administrated to mice by IP injection (10 μL/g of weight) in order to measure cell proliferation. Two hours after IP injection mice were sacrificed by CO<sub>2</sub> inhalation and eyeballs were enucleated and fixed for 16 hours in Davidson's fixative. The cornea was separated from the rest of the eye by scissors. EdU was detected by the Click-iT EdU Imaging Kits (Invitrogen, Paris, France). Cornea was incubated for 4 hours in PBSGT (0.5% Triton X-100) buffer, washed twice in PBS-Tween and incubated with EdU revealing solution for 30 minutes at RT in the dark. Cornea was washed three times for 10 minutes with PBS-Triton 0.1%. Nuclei were stained with TO-PRO-3 a far red-fluorescent nuclear counterstain (ThermoFisher Scientific).

### 2.3.9 | Cornea clearing and imaging

We used the 3DISCO clearing procedure.<sup>33</sup> Corneas were first dehydrated in a graded series of tetrahydroflurane (THF; Sigma-Aldrich, Saint-Quentin Fallavier, France) diluted in H<sub>2</sub>O (THF 50%

overnight, THF 80% for 1 hour, and two times with THF 100% for 1 hour). This was followed by a delipidation step of 30 minutes in dichloromethane 100% (DCM; Sigma-Aldrich). Finally, corneas were cleared overnight in dibenzylether (DBE; Sigma-Aldrich). 3D imaging was performed with an ultramicroscope (LaVision BioTec) and movies were generated using the Imaris x64 software (version 7.6.1, Bitplane).

## 2.4 | Stem cell therapy after corneal opacity development

### 2.4.1 | Isolation and culture of human and mouse corneal SSCs

HSSC: Donor tissue consisted of either corneo-scleral rims obtained during surgery after 8-mm trephination of the graft or corneal grafts discarded during storage due to low endothelial cell counts. All tissues were processed by the Cornea Bank of the French blood institution (Etablissement Français du Sang—Ile-de-France, Paris, France). For corneal grafts, an 8-mm trephination was performed to isolate corneo-scleral rims. Six human donor male (five) and female (one) corneas were used to grow stem cells. The donor age ranged from 48 to 89 years with an average of 74 years.

Superficial limbal explants were prepared under a laminar flow. A stromal dissection between the anterior and mid-stroma was carried out using a 15° blade and the sclera was carefully removed with scissors, resulting in superficial limbal rims that included limbal epithelium and superficial limbal stroma.<sup>34</sup> Two pools of human stem cells grown from three corneas each were used (ie, cultured cells from 3 corneas were pooled and then injected in six murine corneas). The number of cells obtained from one human cornea after sphere dissociation at the end of primary culture ranged from  $1.5 \times 10^6$  to  $2 \times 10^6$ .

MSSC: Four-week-old C57BL/6 mice, three males and three females, were used to obtain MSSC. After mouse sacrifice by CO<sub>2</sub> inhalation, the eyeball was enucleated and the cornea was separated from the rest of the eye using scissors. The number of cells obtained from one mouse cornea after sphere dissociation at the end of primary culture ranged from  $4 \times 10^5$  to  $5 \times 10^5$ .

The human superficial limbal rims and mouse corneas obtained were scraped with a scalpel to remove the limbal epithelium. The rims and mouse corneas were then cut into small pieces and incubated overnight at 37°C in 500 µL of basal medium for human rims and 4 hours at 37°C in 100 µL of basal medium for mouse corneas. The basal medium consisted of Dulbecco's modified Eagle's medium (DMEM; Life Technologies, Courtaboeuf, France) containing 1 mg/mL collagenase A (Sigma-Aldrich). Samples were then centrifuged and the supernatant was removed. One milliliter of DMEM was added and samples were centrifuged a second time followed by removal of the supernatant. Tissue debris was removed by filtration with a 100 µm-pore diameter Macs SmartStrainers (Miltenyi Biotec, Paris, France). After centrifugation at 800g for 5 minutes, the cells were resuspended in DMEM and counted with a hemocytometer. The isolated limbal cell

suspensions were cultured in Essential 8 (E8) medium with no feeders. E8 medium is a xeno-free and feeder-free medium especially formulated for the growth and expansion of human pluripotent stem cells.<sup>35,36</sup> It is made of DMEM/F12, L-ascorbic acid, selenium, transferrin, NaHCO<sub>3</sub>, insulin, FGF2, and TGFβ1. The medium was supplemented with 1.5% methylcellulose gel matrix to prevent reaggregation of isolated cells.<sup>16</sup> The seeding cell density was 4000 cell/cm<sup>2</sup> cultured in 12-well culture plate and cells were grown for 21 days at 37°C under 5% CO<sub>2</sub>. The culture medium was changed three times a week.

Human and mouse SSC were characterized by sphere formation, expression of Pax6, Sox2, Bmi1, Nestin, ABCG2, Keratocan, Vimentin, Sox9, Sox10, and HNK1, absence of P63α, CK14, CK15, and CK3 expression, high growth rate, and the ability to differentiate into various cell lineages, including keratocytes, myo/fibroblasts, neurons, osteocytes, chondrocytes, and adipocytes, with no epithelial differentiation potential as previously reported.<sup>16</sup> These are features of corneal SSCs as opposed to limbal epithelial stem cells.<sup>16</sup>

### 2.4.2 | SSC labeling prior to injection

After 21 days of culture, SSC spheres were dissociated using collagenase A 0.5 mg/mL for 10 minutes at 37°C. Cells were washed with DMEM containing 10% FBS and, after centrifugation at 800 rpm for 5 minutes, they were resuspended in DMEM/F-12 at  $1 \times 10^6$  cells/mL. Cells were pre-labeled with the membrane dyes Vybrant DiO (Invitrogen, Villebon sur Yvette, France). DiO was added to cell suspension at a dilution of 50 µg/mL. Cells were incubated with DiO for 20 minutes at 37°C. They were washed twice with DMEM/F-12 and resuspended in serum-free DMEM/F-12 at  $1 \times 10^4$  cells per 5 µL for injection.

Cells were cultured with Click-iT EdU labeling solution prior to injection. After tissue digestion, cells were suspended in E8 culture medium supplemented with 10 µM of EdU. Cells were incubated and the medium composed of E8 medium and 10 µM of EdU was changed every 2 days. After 3 weeks of culture, cells were harvested and dissociated. Cell suspension was then resuspended in serum-free DMEM/F-12 at  $1 \times 10^4$  cells per 5 µL for injection. One day and 1 month after injection, mice were sacrificed and EdU-positive cells were detected as described above.

### 2.4.3 | SSC injection in the mouse model of corneal opacity

Cell suspensions containing  $1 \times 10^4$  cells per 5 µL in DMEM/F-12 buffer were injected with a 10 µL Hamilton microsyringe (Dominique Dutscher, Issy-les-Moulineaux, France) connected to a 33-gauge glass microcapillary (Dominique Dutscher).

For MSSC injection experiments, 3 weeks after N<sub>2</sub> injury to both right and left eyes of 16 mice, mice were first anesthetized by 5% isoflurane inhalation for 5 minutes and they were maintained in deep

anesthesia with 2% isoflurane inhalation. One drop of a local anesthetic (oxybuprocaine; Thea) was instilled on the corneal surface of both eyes. Right eyes were injected with MSSCs and left eyes with sham consisting of 5  $\mu$ L of DMEM/F-12 medium. Surgery was performed under an operative microscope (Leica F18). A microsyringe containing 5  $\mu$ L of cell suspension or sham was inserted into the central zone of the cornea. Then, the microcapillary was slowly advanced into the stromal space where the cell suspension was injected.

For HSSC injection experiments, 3 weeks after N<sub>2</sub> injury to left eyes of 12 mice, mice were anesthetized and left eyes were injected either with HSSCs (4 mice) or with sham (4 mice) or were not injected (4 mice).

#### 2.4.4 | In vivo imaging

Mice were observed 4 hours after injection with in vivo fluorescence microscopy (Micron III) to monitor the presence of injected DiO-labeled cells in the corneal stroma. Mice were then observed at different time points (ie, at 1 week, 2 weeks, and 1, 2, and 3 months) in vivo with slit lamp, IVCM, and SD-OCT, and ex vivo with FFOCM and histology.

#### 2.4.5 | In vivo fluorescence microscopy

Mice were anesthetized and placed on the Micron III (Phoenix Laboratories). The camera and eye position was adjusted ensuring correct alignment and focus on the surface of the cornea using standard color fundus photography before adjusting to the appropriate filter set for fluorescence imaging. Images were captured using the Streampix software (Phoenix Research Laboratories) as XGA resolution (1024  $\times$  768 pixels) 24-bit RGB sequential tiff files with the Micron III light source at maximum intensity and gain setting of +4 db. Images were taken 4 hours after labeled SSC injection and 1 week, 2 weeks, and 1, 2, and 3 months after injection.

#### 2.4.6 | Histology and immunofluorescence

Three months after cell injection, mice were sacrificed by CO<sub>2</sub> inhalation, and the eyeballs were enucleated and fixed for 16 hours in Davidson's fixative. Eyeballs were included in paraffin and frozen. Immunostaining was performed on paraffin embedded sections. Eyeballs were cut in 5- $\mu$ m-thick sections with a microtome (Leica RM2145; Leica, Paris, France). Sections were collected on slides (Superfrost; Thermo Scientific), immersed in histosol and rehydrated in 100%, 90%, and 70% ethanol and double-distilled water. Sections were stained with hematoxylin and eosin stain (HE) to enhance nucleus visualization and mounted. Light microscope images of stained sections were scanned with the Hamamatsu 174 NanoZoomer Digital Pathology (NDP) 2.0 HT (Hamamatsu Photonics, Massy, France).

Sections on slides were subjected to immunostaining after rehydration. They were incubated for 1 hour in PBS containing 0.3% Triton X100 and 0.2% gelatin (PBSGT) to block nonspecific binding. Sections were then incubated overnight at 4°C with primary antibodies diluted in PBST. After washing in PBS, sections were incubated for 1 hour at RT with the appropriate secondary antibodies diluted in PBST: Alexa Fluor 488 IgG (1:500) and Alexa Fluor 594 IgG (1:500) antibodies (Sigma). Nuclei were stained with Dapi (11 000; Molecular Probes). Cells were washed three times, 5 minutes each with PBST followed by mounting with fluoromount-G (Clinisciences, Nanterre, France).

Primary antibodies used were: anti-Ki67 (1/200, 550609, BD Pharmingen, Le Pont de Claix, France), monoclonal anti- $\alpha$ -SMA antibody (1/200, A2547, Sigma-Aldrich) and anti-collagen type III (1/100, ab7778, Abcam, Paris, France), anti-Laminin antibody (1/200, ab11575, Abcam), anti-CD31 (1/200, SL31, Dianova, Hamburg, Allemagne).

Stained samples were observed with an Olympus FV1000 laser-scanning confocal microscope (Olympus, Rungis, France). Twelve-bit images were processed with ImageJ, where Z-sections were projected on a single plane using the maximum intensity option under the Z-project function. Images were finally converted into 24-bit RGB color mode and figures were then assembled.

#### 2.4.7 | Scanning electron microscopy analysis

Eight corneas (three control, three N<sub>2</sub> injured, one MSSC-injected, and one sham-injected) were dissected and fixed via careful immersion in a solution of 2.5% (v/v) glutaraldehyde in 0.1 M sodium cacodylate buffer pH 7.2 at RT. They were then washed three times for 5 minutes with 0.1 M sodium cacodylate buffer and dehydrated with increasing concentrations of ethanol at RT (50-70-90%, 3  $\times$  100%, v/v with ultrapure water) for 10 minutes at each step. After immersion in acetone and epoxy resin, samples were placed in flat molds (allowing positioning for precise transversal sectioning) and polymerization was performed by incubation for 72 hours at 60°C. Ultrathin sections of 70 nm were cut with an UCT ultramicrotome (Ultracut, Leica microsystems) and deposited on 200 mesh copper grids (Electron Microscopy Sciences). Observations were performed using an LaB<sub>6</sub> JEM 2100 HC transmission electron microscope (Jeol, Croissy sur seine, France), at 120 kV and with an objective aperture adjusted for each sample and magnification.

### 2.5 | Statistical analysis

Statistical analysis was performed using Prism 7 (GraphPad software) with appropriate statistical tests including the Mann-Whitney test, one-way and two-way analysis of variance, or the Kruskal-Wallis test followed when necessary by a multiple comparison test (post hoc analysis). *P*-values <.05 were considered statistically significant.

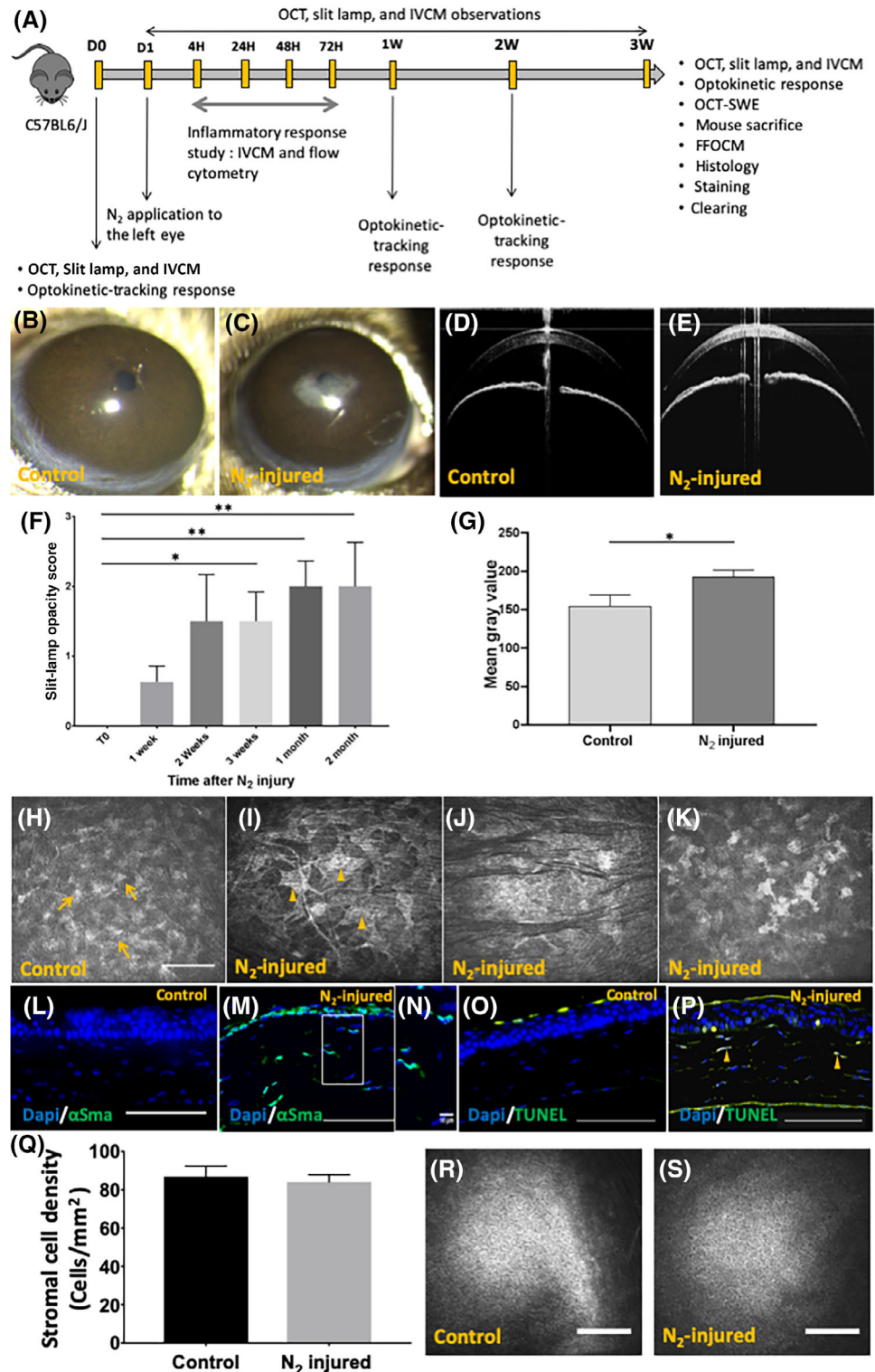
### 3 | RESULTS

#### 3.1 | Corneal opacity mouse model development

Forty-four 4-week-old C57BL/6 mice were used for the development of the corneal opacity mouse model. After epithelial debridement, N<sub>2</sub> was applied to the left eye of each mouse. Mice were assessed in vivo

with slit lamp, OCT, and IVCM (Figure 1). Slit-lamp observation demonstrated the development of a haze in the center of the left cornea 3 weeks after application of N<sub>2</sub> (Figure 1C) with increased corneal reflectivity evidenced by OCT (Figure 1E) in all animals. The cornea of the right (control) eye remained transparent (Figure 1B,D). Semi-quantitative (Figure 1F) analysis of corneal transparency demonstrated a significant increase ( $P = .01$ ) in slit-lamp opacity score

**FIGURE 1** Corneal opacity mouse model development. A, Schematic representation of corneal mouse model development study. Forty-four mice: development of the corneal opacity mouse model. Twenty-six mice: slit lamp for days 0 to 3 months. IVCM and OCT. Sixteen mice: inflammatory response analysis. Two mice: clearing experiment. B,D, Slit-lamp and OCT observations of control (right eye) mouse corneas. C,E, Slit-lamp and OCT observations after 3 weeks of N<sub>2</sub>-injured mouse corneas (left eye). F, Slit-lamp opacity score calculated 3 weeks after N<sub>2</sub> application. G, Mean gray value of OCT cross sections determined by the ImageJ software. H-K, IVCM images of normal cornea (H) and N<sub>2</sub>-injured cornea (I, J, K). Unremarkable keratocytes can be observed in normal cornea (H, arrow) and myofibroblasts (I, arrowhead), hyporeflexive striae (J), and nucleus condensation (K) in injured cornea 3 weeks after N<sub>2</sub> application. L,M, Immunofluorescence staining of  $\alpha$ -SMA in control (L) and injured (M, N) cornea. O,P, TUNEL test in normal cornea (O) and injured cornea (P). Arrowheads show apoptotic stromal cells (P). Q, Stromal cell density was assessed from images obtained with IVCM in 44 mice. R,S, Normal endothelial appearance in control and N<sub>2</sub>-injured corneas. Scale bars = 100  $\mu$ m. Error bars =  $\pm$ SEM. \* $P < .05$ ; \*\* $P < .01$ .  $\alpha$ -SMA, alpha-smooth muscle actin; IVCM, in vivo confocal microscopy; OCT, optical coherence tomography





obtained after N<sub>2</sub> application in comparison with that in control cornea. Compared with baseline, the opacity score was significantly increased at 3 weeks, and 1 and 2 months, whereas the increase in the opacity score at 1 and 2 weeks was not significant. Quantitative analysis (Figure 1G) of corneal backscattering assessed with OCT images demonstrated a significant increase ( $P = .01$ ) in the level of backscattering of the left cornea 3 weeks after N<sub>2</sub> application in

comparison with the control eye. IVCM done 3 weeks after N<sub>2</sub> application revealed, in comparison with control cornea (Figure 1H), the presence of hyperreflective enlarged stromal cells (Figure 1I) of a myofibroblast appearance. In addition, immunofluorescence analysis showed the presence of  $\alpha$ -SMA positive cells in N<sub>2</sub>-injured stroma (Figure 1M,N). Nucleus condensation observed with IVCM (Figure 1K) was associated with the presence of apoptotic cells identified by a

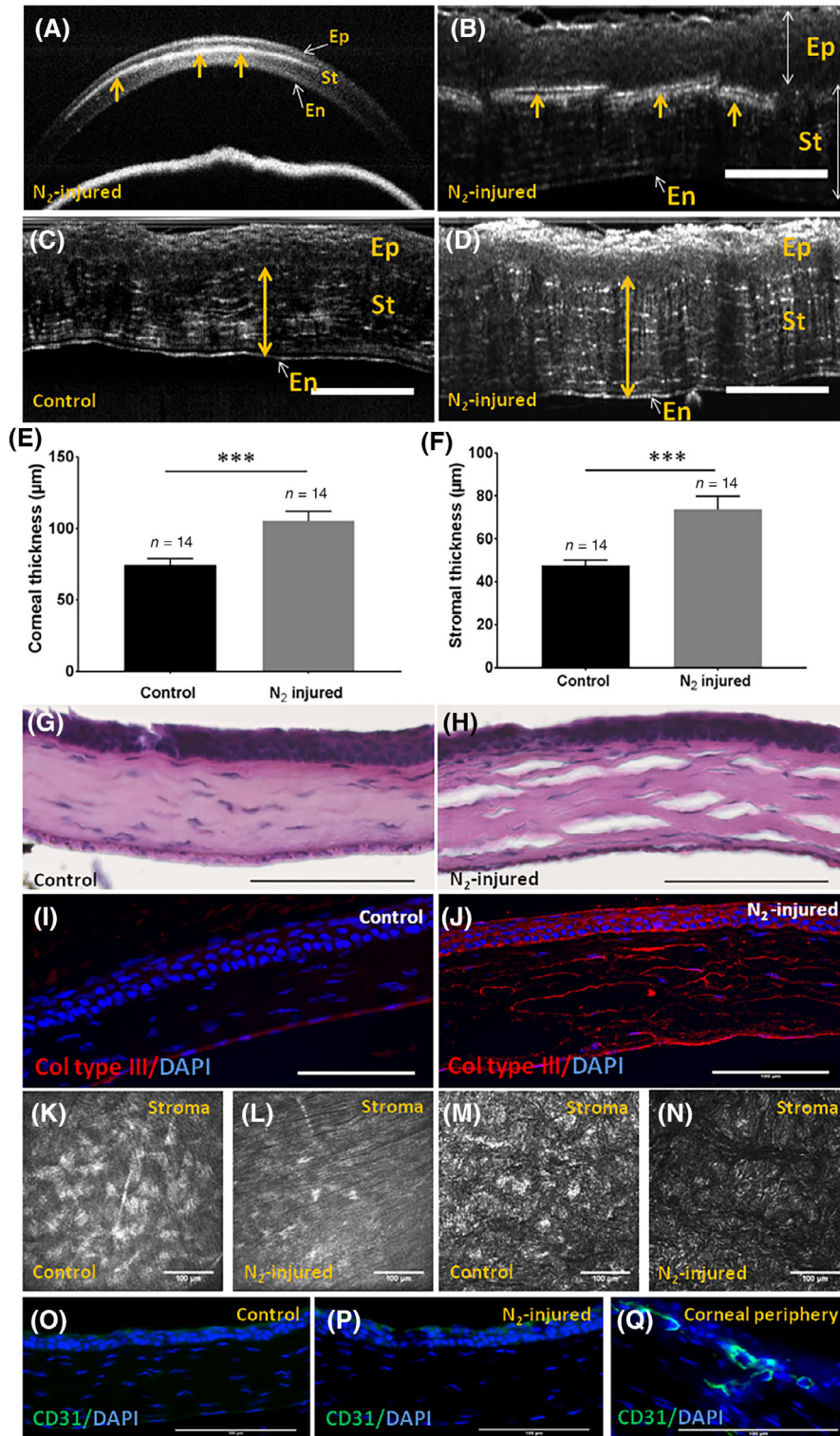


**FIGURE 2** Corneal stromal characterization 3 weeks after liquid nitrogen application. A,B, OCT and FFOCM cross sections of N<sub>2</sub>-injured cornea, respectively. Arrows show the presence of an opaque zone in corneal stroma. C,D, FFOCM images used to determine corneal stromal and total corneal thicknesses with the ImageJ software before (C) and 3 weeks after N<sub>2</sub> application (D). E,F, Corneal and stromal thicknesses were significantly higher ( $P = .0004$ ) in injured vs control corneas 3 weeks after N<sub>2</sub> application. G,H, Histological analysis with hematoxylin and eosin staining of control and N<sub>2</sub>-injured corneas, respectively. I,J, Immunofluorescence analysis for collagen type III, in control vs N<sub>2</sub>-injured corneas. K,L, IVCM images of normal (K) and N<sub>2</sub>-injured (L) cornea showing the absence of blood vessel in corneal stroma. M,N, FFOCM en face images of normal (M) and N<sub>2</sub>-injured (N) cornea showing the absence of blood vessel in corneal stroma. O-Q, CD31 negative staining in normal (O) and N<sub>2</sub>-injured (P) cornea. Positive CD31 staining was observed in corneal periphery (Q). Scale bars = 100  $\mu\text{m}$ . Error bars =  $\pm$ SEM. \*\*\* $P < .001$ . FFOCM, full field optical coherence microscopy; IVCM, in vivo confocal microscopy; OCT, optical coherence tomography

TUNEL test (Figure 1P). Neither apoptotic cells nor  $\alpha$ -SMA positive cells were observed in control cornea (Figure 1L,O). The morphology of stromal striae was modified in treated cornea where they looked hyporeflexive and surrounded by hyperreflexive ECM (Figure 1J). Mean stromal cell density assessed with IVCM in control cornea was  $87 \pm 37$  cells/mm<sup>2</sup>. Three weeks after N<sub>2</sub> application, this figure was  $84 \pm 25$  cells/mm<sup>2</sup>. The mean stromal cell density was not modified by N<sub>2</sub> application (Figure 1Q). No changes in endothelial cell morphology in control (Figure 1R) and N<sub>2</sub>-injured (Figure 1S) corneas were observed 3 weeks after N<sub>2</sub> application.

### 3.2 | Corneal stromal characterization

Both OCT (Figure 2A) and FFOCM (Figure 2B) showed that the opacification was located in the anterior part of the corneal stroma of injured eyes. Corneal (Figure 2E) and stromal (Figure 2F) thicknesses assessed with FFOCM were significantly higher in injured vs control corneas 3 weeks after N<sub>2</sub> application. Histological analysis with HE staining revealed dissociation of collagen lamellae in corneal stroma after N<sub>2</sub> application (Figure 2H), but not in control corneas (Figure 2G). Immunofluorescence analysis showed stronger staining for collagen type III in injured (Figure 2J) compared with control (Figure 2I) corneas. Last, no corneal vascularization was observed with IVCM (Figure 2K,L), FFOCM (Figure 2M,N), and histology in both N<sub>2</sub> injured (Figure 2L,N), and control corneas (Figure 2K,M).

### 3.3 | Epithelial layer before and after N<sub>2</sub> application

Epithelium examination by slit lamp after fluorescein eyedrop instillation was unremarkable in control cornea (Figure S2A,B). It revealed the presence of an epithelial defect in the central zone of the injured cornea 4 hours after N<sub>2</sub> application (Figure S2C). The epithelial defect resolved 48 hours after N<sub>2</sub> application (Figure S2D). IVCM observations revealed the presence of the three corneal epithelial layers (ie, superficial [Figure S2E], intermediate [Figure S2F], and basal [Figure S2G]) in control cornea. In the injured cornea 3 weeks after N<sub>2</sub> application, superficial cells were observed with no evident borders (Figure S2H). Intermediate (Figure S2I) and basal cells (Figure S2J) appeared hyperreflexive, with basal cells featuring strongly hyperreflexive cell borders.

HE staining showed the presence of the three different layers of the corneal epithelium as did IVCM in the control cornea (Figure S2K). Conversely, organization of the corneal epithelium including stratification and cell morphology was poorly defined in injured cornea (Figure S2L). A high number of EdU-positive epithelial basal cells were observed after N<sub>2</sub> injury (Figure S2N, Movies S2) compared with control cornea (Figure S2M, Movie S1). FFOCM cross sections showed the absence of the epithelial basement membrane in the injured cornea (Figure S2P) compared with the control (Figure S2O) as did TEM (Figure S2Q,R) and Laminin staining (Figure S2S,T). Significant

differences ( $P = .02$ ) in epithelial thickness obtained with FFOCM images were observed between injured and control eyes (Figure S2U) with higher epithelial thickness for the injured corneas.

### 3.4 | Inflammatory response development

An inflammatory response was observed by IVCM and flow cytometry analysis after N<sub>2</sub> application (Figure 3). Hyperreflexive, round, small cells were observed in vivo 4 and 24 hours after N<sub>2</sub> application, corresponding to the presence of inflammatory cells in the anterior corneal stroma (Figure 3A). This finding was observed in corneal cross sections stained with HE (Figure 3B). Arrowheads in Figure 3B show polynuclear cell infiltration in corneal stroma after N<sub>2</sub> injury. The upper level of CD11b-positive cells was measured to be 48.6% 4 hours after N<sub>2</sub> application by flow cytometry. This figure decreased to 15.5% 24 hours after injury. Inflammatory cells were not observed in vivo beyond 24 hours after injury, but were detected by CD11b staining with an average of 13.45% 48 hours and 6.4% 72 hours after injury (Figure 3C).

### 3.5 | Corneal biomechanics and visual acuity

Three weeks after N<sub>2</sub> application, a slow shear wave speed corresponding to the red colors (Figure 4B) was obtained for the control eyes. High shear wave speed (yellow colors) was observed for the N<sub>2</sub>-injured cornea (Figure 4C). The mean shear wave speed measured was significantly higher ( $P = .009$ ) in N<sub>2</sub>-injured cornea compared with that in control cornea (Figure 4D).

Visual acuity of 12 mice was assessed before and 1, 2, and 3 weeks after N<sub>2</sub> application to the left eyes. Analysis was performed with an optometry system. Figure 4E shows the OTR obtained for the right eye. No significant differences were observed before and after each postapplication time for the control eye (D 0,  $0.354 \pm 0.017$ ; 1 W,  $0.346 \pm 0.008$ ; 2 W,  $0.341 \pm 0.012$ ; 3 W,  $0.344 \pm 0.015$ ) (mean  $\pm$  SEM). Mean OTR of the left eye before N<sub>2</sub> application (Figure 4F) was  $0.361 \pm 0.016$ . This mean value significantly decreased 1 week ( $0.282 \pm 0.033$ ;  $P = .0005$ ), 2 weeks ( $0.283 \pm 0.069$ ;  $P = .0005$ ), and 3 weeks ( $0.302 \pm 0.073$ ;  $P = .001$ ) after N<sub>2</sub> application.

### 3.6 | Injection of HSSC and MSSC in corneal opacity mouse model

Human and mouse corneal SSCs were cultured for 3 weeks in xeno-free and feeder-free medium and characterized as previously described.<sup>16</sup> SSCs were prelabeled with the membrane dye Vybrant DiO or with EdU to follow injected SSC in mouse cornea with in vivo and ex vivo fluorescence imaging. Three weeks after N<sub>2</sub> application, HSSCs or MSSCs ( $1 \times 10^4$  cells per 5  $\mu$ L) were injected in mouse corneal stroma. Mice were observed 1 day, and 1, 2, and 3 months after injection.



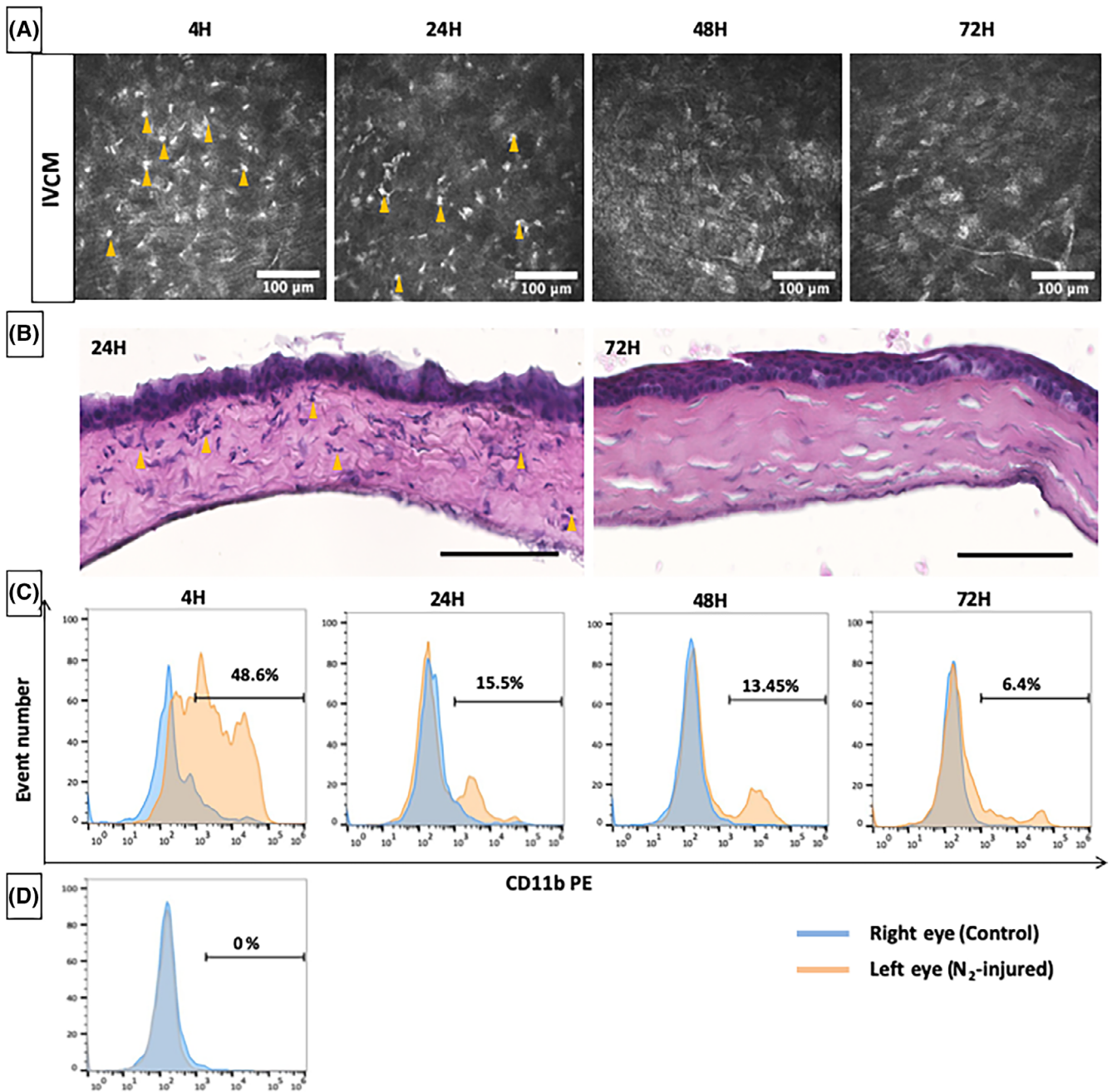


**FIGURE 3** Inflammatory response after liquid nitrogen injury. A, in vivo confocal microscopy (IVCM) images obtained 4, 24, 48, and 72 hours after liquid nitrogen application. Arrowheads show inflammatory cells in corneal stroma. Scale bars = 100  $\mu$ m. B, Hematoxylin and eosin staining of corneal cross sections 24 and 72 hours post-N<sub>2</sub> application. Arrowheads show polynuclear cell infiltration. Scale bars = 100  $\mu$ m. C, Flow cytometry plot of cell suspensions obtained after corneal dissociation of right (blue) and left (red) eye after liquid nitrogen application. CD11b-positive cells decrease with postapplication time. D, Flow cytometry plot of cell suspension obtained from control mice

Figure 5B shows in vivo fluorescence imaging demonstrating the presence of densely packed DiO-labeled HSSC and MSSC in mouse cornea 1 day after injection. Both human and murine spreading SSCs were observed at 1 month, featuring weaker staining. We observed the presence of injected labeled HSSC 2 and 3 months after injection. Conversely, labeled MSSCs were not found 2 and 3 months after injection. One day after injection, confocal microscopy showed the presence of DiO-labeled (Figure 5C)

and EdU-positive (Figure S3A) SSCs in the injected site. One month later (Figure 5D), some DiO-labeled cells were still in the injected site (Figure 5E), whereas others had migrated in the corneal stroma (Figure 5F). This finding was confirmed by the presence of EdU-positive cells far from the injected site (Figure S3B). Cross sections showed the presence of injected cells in the corneal stroma (Figure 5G), mainly located between two adjacent stromal lamellae. The same feature was observed with OCT, which showed the

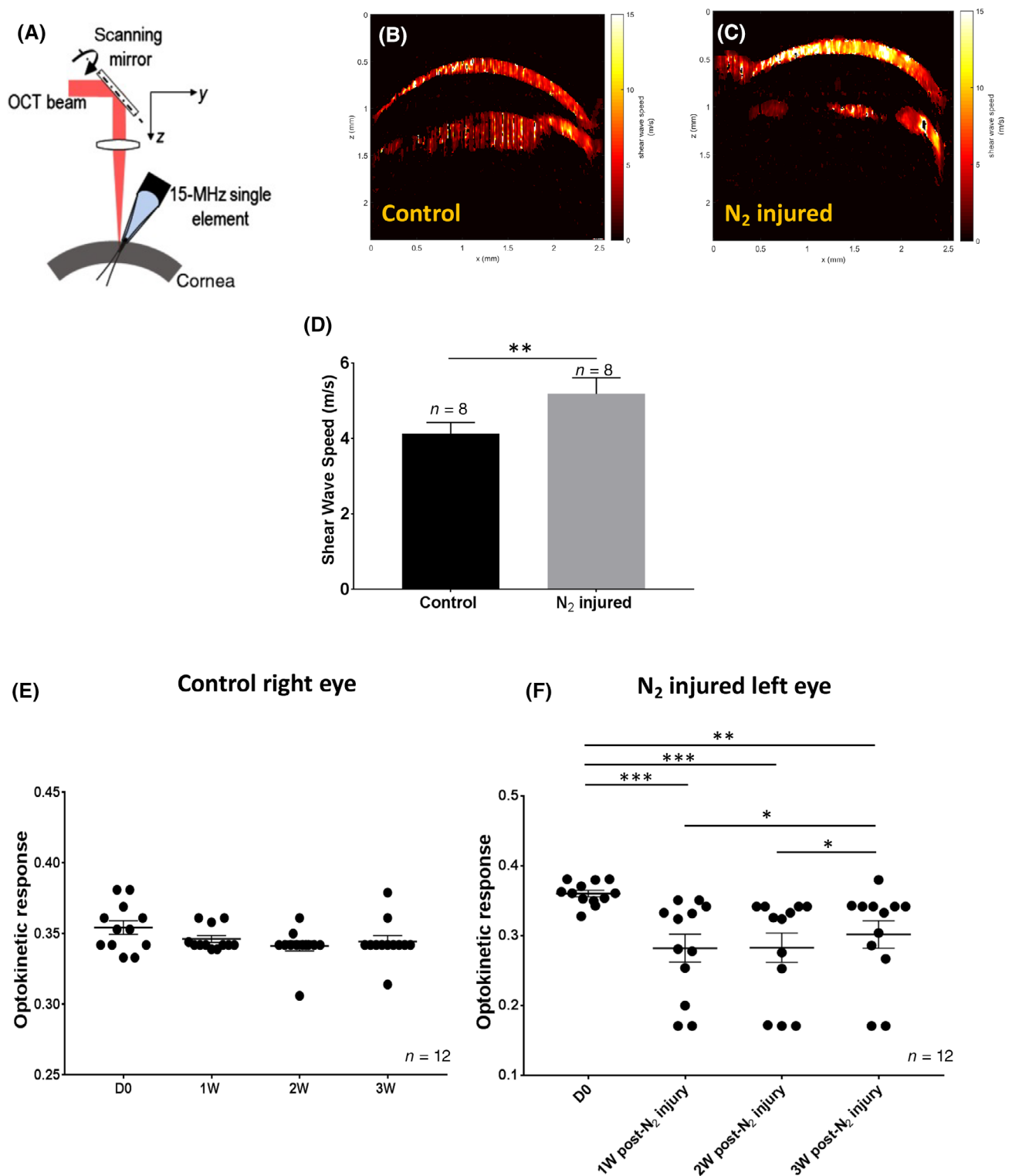


**FIGURE 4** Optical coherence elastography (OCE) and optokinetic tracking response (OTR) measurements. A, Schematic representation of the optical coherence tomography shear wave elastography system. B,C, Images obtained with OCE in the right (control) and left (N<sub>2</sub> injured) corneas. The red color (B) corresponds to a slow shear wave speed and the yellow (C) to a high shear wave speed. D, The shear wave speed was significantly higher in the injured corneas compared with the control ones ( $P = .008$ ) 3 weeks after N<sub>2</sub> application. E,F, OTR measured in the control eye (E, right eye) and in the N<sub>2</sub>-injured eye (F, left eye) before and after each postapplication time. Error bars =  $\pm$ SEM. \* $P < .05$ ; \*\* $P < .01$ ; \*\*\* $P < .001$

hyperreflective zone to be formed just after injection (arrowhead, Figure 5H), and with FFOCM showing hyperreflective cells (arrowhead, Figure 5I) located in a unique corneal stromal plane. Injected

cells were also observed in the corneal stroma with IVCM featuring hyperreflective nuclei (Figure 5K). These cells were not detected in noninjected corneas (Figure 5J).

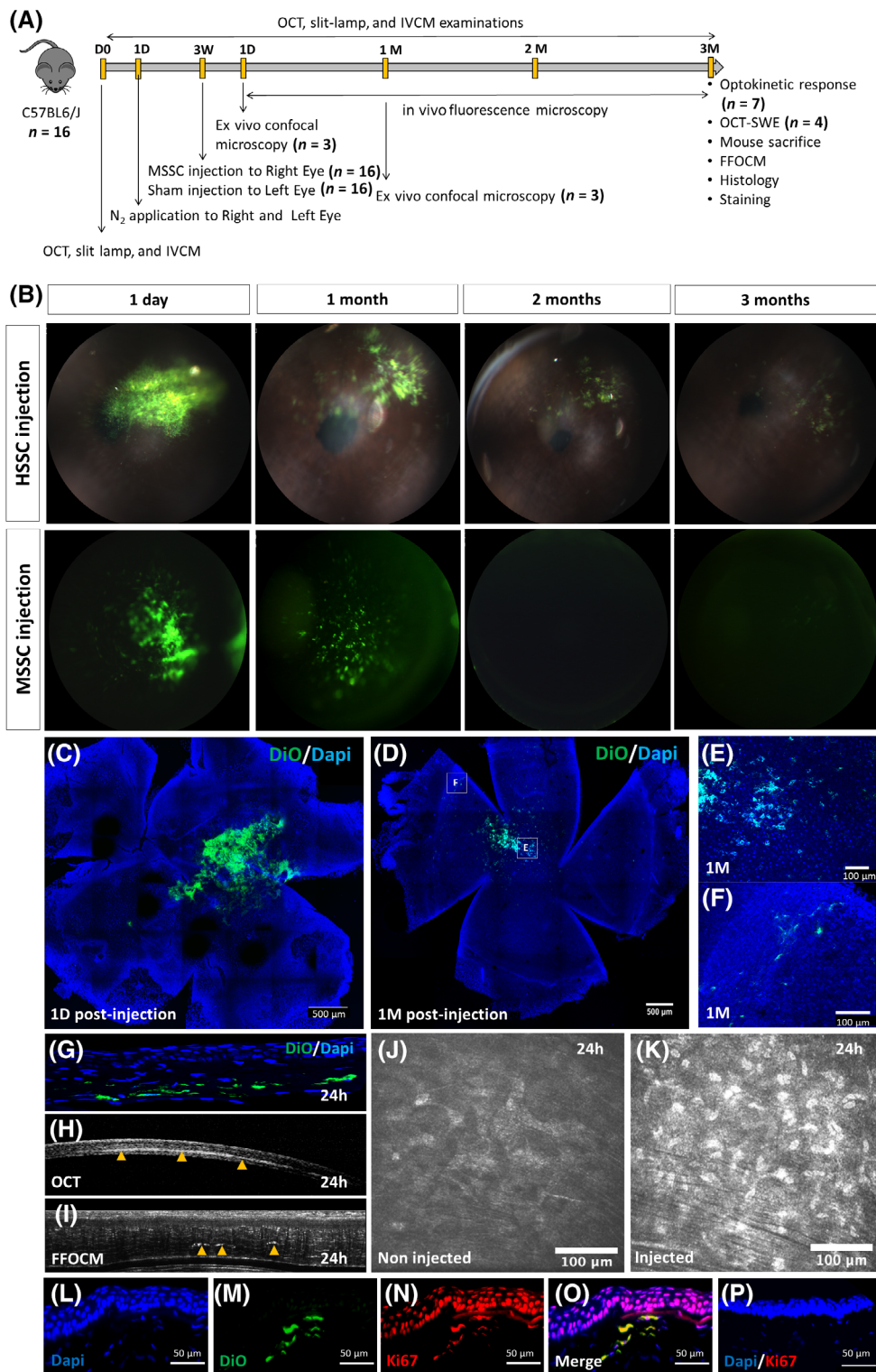


**FIGURE 5** Injection of HSSC and MSSC in corneal opacity mouse model. A, Schematic representation of MSSC injection after N<sub>2</sub> injury. B, in vivo imaging of N<sub>2</sub>-injured corneas injected with HSSC or MSSC 1 day, 1, 2, and 3 months after injection. C-F, Confocal microscopy showing the presence of injected DiO-labeled SSC in the cornea 1 day (C) and 1 month (D, E, F) after injection. G-I, Corneal cross sections obtained by histology (G), OCT (H), and FFOCM (I) showing the presence of injected cells (green cells [G] and arrowhead [H, I]) in the corneal stroma. J,K, En face images obtained by IVCM in N<sub>2</sub>-injured noninjected (J) and N<sub>2</sub>-injured SSC-injected cornea (K). L-O, DiO-labeled cells (M) featuring positive staining for Ki67 (N, O). P, Negative Ki67 staining for epithelial and stromal cells far from the injected site. FFOCM, full field optical coherence microscopy; HSSC, human stromal stem cell; MSSC, mouse stromal stem cell; OCT, optical coherence tomography; SSC, stromal stem cell

One month after injection, DiO-labeled cells (Figure 5M) showed positive staining for Ki67, showing that they were dividing (Figure 5N). Epithelial cells above the DiO-labeled cells were found to be positive for Ki67 staining (Figure 5N,O), demonstrating a paracrine effect of SSC-injected cells. Epithelial cells that were far from the injection site and for control cornea were negative for Ki67 staining (Figure 5P).

### 3.7 | Epithelial and stromal characterization after MSSC injection

Sixteen mice were injected with murine SSC. Three months after injection, the three corneal epithelial layers were observed in the MSSC- (Figure 6D-F) and sham-injected (Figure 6A-C) corneas with IVCM. The superficial layer was still hyperreflective after sham injection (Figure 6A).



Intermediate (Figure 6B,E) and basal cells (Figure 6C,F) appeared to be normal in both MSSC- and sham-injected corneas. Epithelial, stromal, and corneal thicknesses calculated with FFOCM images (Figure 6K) were similar in the two conditions. In sham-injected cornea, HE staining showed that collagen lamellae were dissociated (Figure 6I) in comparison with MSSC-injected cornea (Figure 6J) where collagen lamellae featured a normal aspect with few lamellar dissociations. Morphology of stromal striae was still modified in sham-injected cornea where they looked

hyporeflective (Figure 6M). Stromal striae were not visible 3 months after MSSC injection (Figure 6O). The endothelium appeared to be not modified in either sham- (Figure 6N) or MSSC-injected (Figure 6P) corneas. Stromal cell density was significantly increased in MSSC-injected cornea in comparison with N<sub>2</sub>-injured and control cornea (Figure 6L). Sham-injected cornea featured higher stromal cell density than N<sub>2</sub>-injured cornea. No significant differences in stromal cell density were found between sham- and MSSC-injected corneas (Figure 6L). Both staining for

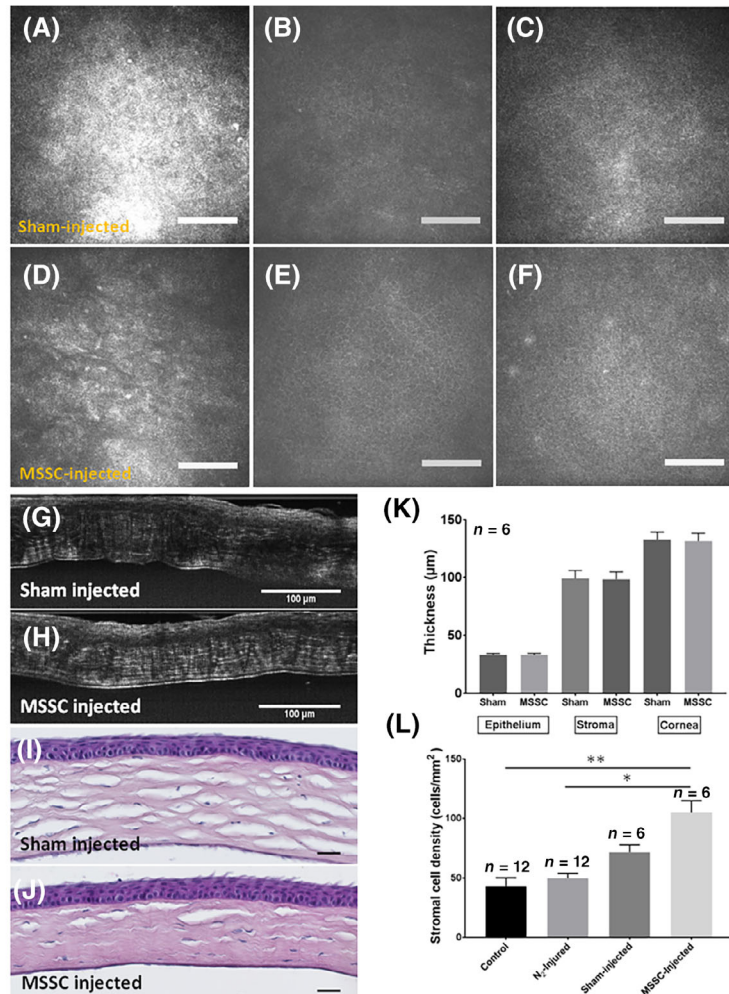
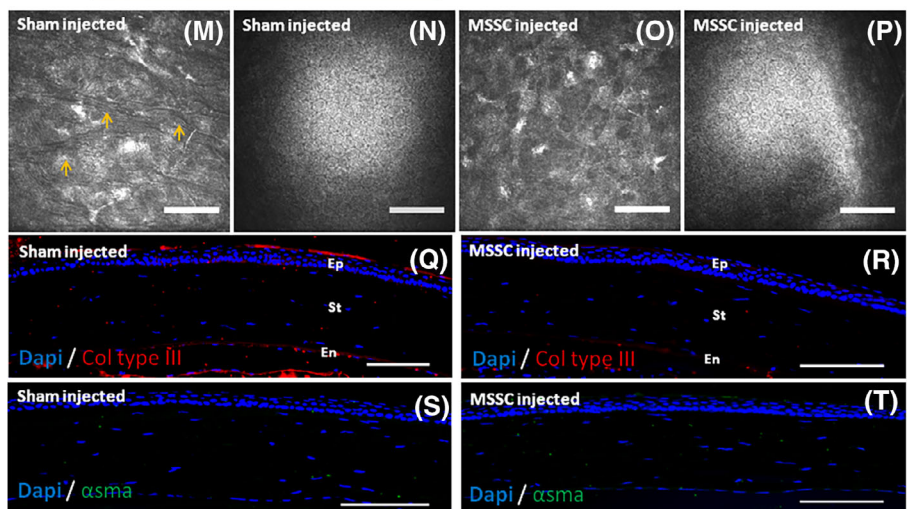


**FIGURE 6** Epithelial and stromal characterization after MSSC injection. A-C, IVCM en face view of the epithelial layer 3 months after sham injection. D-F, IVCM en face view of the epithelial layer 3 months after MSSC injection. G,H, FFOCM cross sections of the cornea after sham (G) and MSSC (H) injections. I,J, Hematoxylin and eosin staining of corneal cross sections after sham (I) and MSSC (J) injections. K, Epithelial, stromal, and corneal thicknesses determined with FFOCM cross sections. L, Stromal cell density calculated with IVCM images 3 months after injection. M,O, IVCM images of the stromal layer. Arrowheads show stromal striae in sham-injected cornea (M). N,P, Normal endothelial appearance in sham- and MSSC-injected corneas. Q,R, Collagen type III staining in both sham- and MSSC-injected corneas. S,T,  $\alpha$ -SMA staining in both sham- and MSSC-injected corneas. Scale bars = 100  $\mu$ m. Errors bars =  $\pm$ SEM; \* $P$  < .05; \*\* $P$  < .01.  $\alpha$ -SMA, alpha-smooth muscle actin; FFOCM, full field optical coherence microscopy; MSSC, mouse stromal stem cell; IVCM, in vivo confocal microscopy



collagen type III (Figure 6Q,R) and  $\alpha$ -SMA (Figure 6S,T) were negative in MSSC and sham-injected corneas.

### 3.8 | Therapeutic effect of MSSC 3 months after injection

By slit-lamp examination, MSSC-injected corneas showed decreased haze 3 months after injection compared with corneas that received a

sham injection and noninjected  $N_2$ -injured corneas (Figure 7A). The corneal opacity score calculated with slit-lamp images (Figure 7B) was significantly higher in  $N_2$ -injured corneas compared with  $N_2$ -injured MSSC-injected corneas ( $P = .008$ ) and control corneas ( $P = .001$ ). No significant differences were observed between corneal opacity scores for  $N_2$ -injured corneas and  $N_2$ -injured sham-injected corneas ( $P = .14$ ). The corneal opacity score for control corneas was significantly lower compared with  $N_2$ -injured MSSC-injected corneas ( $P = .03$ ) and  $N_2$ -injured sham-injected corneas ( $P = .004$ ). Although the corneal

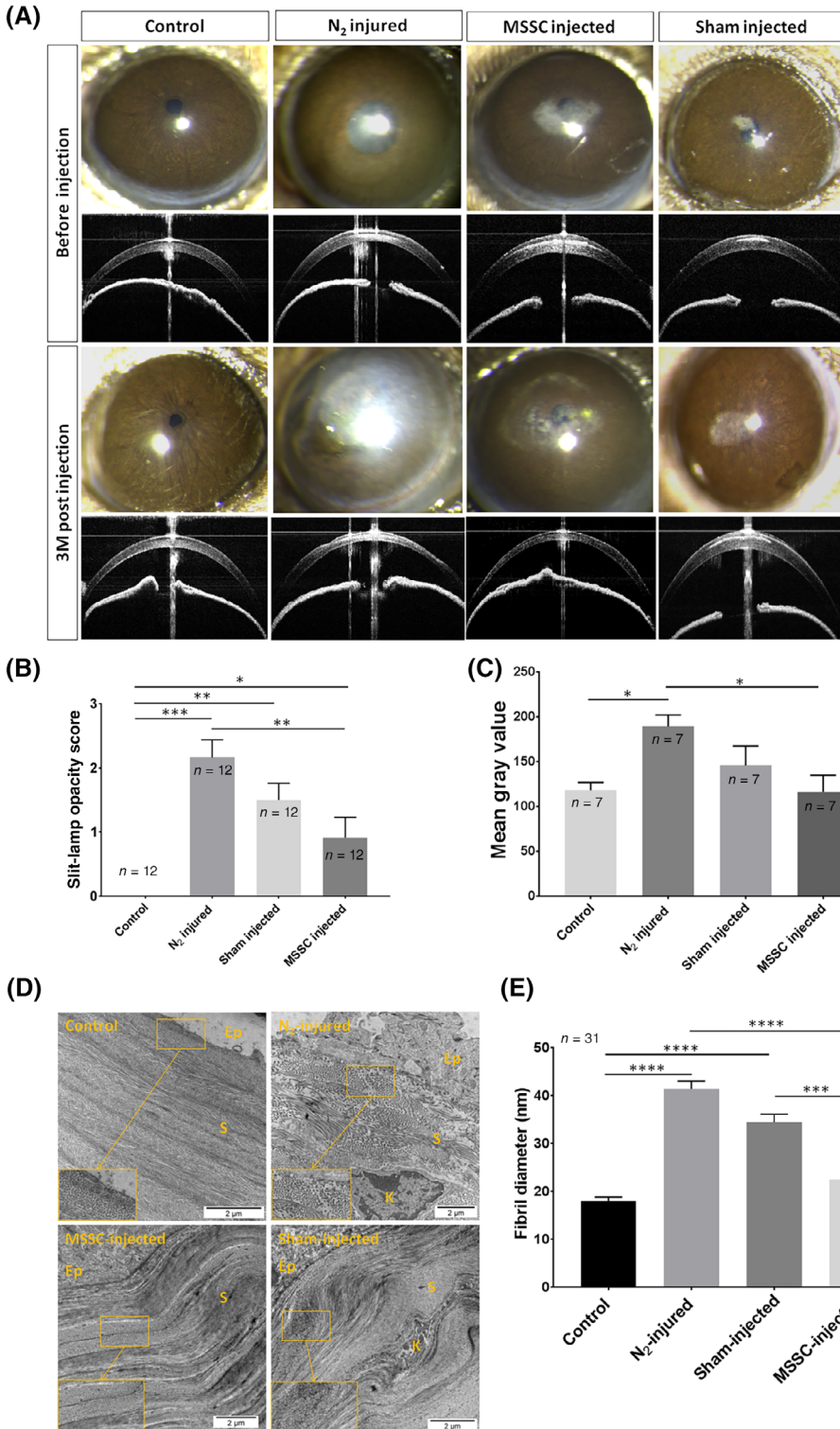


**FIGURE 7** Therapeutic effect of MSSC 3 months after injection. A, Slit-lamp and OCT examination of corneal opacity and hyperreflectivity before and 3 months after  $N_2$  application, MSSC injection, and sham injection. B, Corneal opacity score calculated with slit-lamp images. C, Mean gray value analysis of the OCT cross sections with the ImageJ software. D, TEM images showing ECM organization in control,  $N_2$ -injured, MSSC-injected, and sham-injected cornea. E, Fibril diameter analysis determined with the ImageJ software from TEM images. Eight corneas were analyzed with three images per cornea. For each image 31 fibrils were assessed. Error bars =  $\pm$ SEM. \* $P < .05$ , \*\* $P < .01$ , \*\*\* $P < .001$ , \*\*\*\* $P < .0001$ . ECM, extracellular matrix; MSSC, mouse stromal stem cell; OCT, optical coherence tomography; TEM, transmission electron microscopy

opacity score was lower in N<sub>2</sub>-injured MSSC-injected corneas compared with N<sub>2</sub>-injured sham-injected corneas, the difference did not reach significance ( $P = .22$ ).

OCT cross sections (Figure 7A) showed weaker corneal hyper-reflectivity in N<sub>2</sub>-injured MSSC-injected corneas compared with that in N<sub>2</sub>-injured corneas and N<sub>2</sub>-injured sham-injected corneas. This finding was confirmed by mean gray value analysis of the OCT images with the ImageJ software (Figure 7C). Three months after injection, the mean gray value of N<sub>2</sub>-injured MSSC-injected corneas was significantly lower than that of N<sub>2</sub>-injured corneas ( $P = .03$ ). The mean gray value of N<sub>2</sub>-injured MSSC-injected corneas was lower than that of N<sub>2</sub>-injured sham-injected cornea but still not significant. Conversely, no significant differences were found between N<sub>2</sub>-injured sham-injected corneas and N<sub>2</sub>-injured corneas ( $P = .16$ ).

Collagen in control cornea evidenced by TEM (Figure 7D) was organized into distinct layers containing small, uniform, and tightly packed fibrils. In N<sub>2</sub>-injured cornea, this organization was lost and no tightly packed fibrils were seen. Collagen lamellae were well organized with no obvious differences in the stromal ultrastructure between the control and MSSC-injected corneas. Sham-injected cornea featured better stromal organization compared with N<sub>2</sub>-injured cornea but weaker than MSSC-injected cornea. We found a significant increase in fibril diameters after N<sub>2</sub> injury compared with control cornea ( $18.06 \pm 4.36$  nm vs  $41.48 \pm 8.84$  nm, respectively, [ $n = 31$ ];  $P < .0001$ ) and a significant decrease in fibril diameter ( $22.54 \pm 5.02$  nm) after MSSC injection ( $P < .0001$ ) compared with N<sub>2</sub>-injured cornea (Figure 7E). Fibril diameter was significantly higher ( $34.45 \pm 9.37$ ) in sham-injected cornea than in control ( $P < .0001$ ) and MSSC-injected ( $P = .0002$ ) corneas.

### 3.9 | Therapeutic effect of HSSC

Four mice were injected with HSSC. In addition, four mice were injected with sham, and four were not injected. In N<sub>2</sub>-injured cornea and N<sub>2</sub>-injured sham-injected cornea, the extent of the corneal haze was increased 3 months post-N<sub>2</sub> application and 3 months after sham injection (Figure S4A). N<sub>2</sub>-injured HSSC-injected cornea featured decreased corneal haze (Figure S4A). Slit-lamp opacity score was increased after N<sub>2</sub> injury but decreased after HSSC injection (Figure S4B).

OCT cross sections showed an increase in corneal backscattering in N<sub>2</sub>-injured and sham-injected corneas (Figure S4C). Corneal backscattering was decreased 3 months after HSSC injection (Figure S4C). Stromal cell density obtained with IVCM images was higher after 3 months in N<sub>2</sub>-injured HSSC-injected cornea than in N<sub>2</sub>-injured cornea (Figure S4D).

### 3.10 | Changes in corneal rigidity and vision after MSSC injection

The mean shear wave speed calculated in N<sub>2</sub>-injured MSSC-injected corneas was lower compared with mean shear wave speed in N<sub>2</sub>-injured sham-injected corneas (Figure S5A).

OTR measured in N<sub>2</sub>-injured MSSC-injected corneas was significantly higher than OTR measured in N<sub>2</sub>-injured corneas ( $P = .02$ ; Figure S5B), whereas no significant differences in OTR were observed between N<sub>2</sub>-injured sham-injected corneas and both N<sub>2</sub>-injured corneas and N<sub>2</sub>-injured MSSC-injected corneas. OTR was significantly lower in N<sub>2</sub>-injured corneas compared with that in control corneas ( $P = .02$ ; Figure S5B).

## 4 | DISCUSSION

The aim of our study was to develop a corneal opacity mouse model and to assess the therapeutic effect of corneal SSCs in the restoration of the ECM organization and corneal transparency. Our strategy was to induce a corneal opacity by application of N<sub>2</sub> in mouse cornea after epithelial debridement. SSCs were then injected and their therapeutic effect was monitored.

In our mouse model of corneal opacity, we observed early inflammation after N<sub>2</sub> application that gradually reduced with time. This early inflammatory response was followed by keratocyte apoptosis and keratocyte transformation into myofibroblasts which are common cellular events that occur after corneal injury. These events resulted in late inflammatory response characterized by collagen type III synthesis, corneal stromal haze formation, corneal biomechanical changes including increased corneal rigidity, and impaired visual acuity which are common features of corneal scarring process. SSCs were injected in N<sub>2</sub>-injured cornea at the late phase of inflammation (ie, when fibrotic scar tissue was formed). This intervention resulted in improved corneal transparency associated with SSC migration and growth in the recipient stroma, absence of inflammatory response, recipient corneal epithelial cell growth, increased stromal cell density, absence of myofibroblasts, decreased collagen type III stromal content, decreased stromal haze, decreased corneal rigidity, and improved vision.

### 4.1 | Corneal response to N<sub>2</sub> injury

Keratoconus is a common corneal condition associated with stromal fibrosis in advanced stages.<sup>37</sup> Corneal damage associated with this condition usually occurs in teenagers or young adults.<sup>38-40</sup> Pediatric keratoconus tends to be more aggressive than adult keratoconus because of the dynamic environment in the young cornea.<sup>38,41</sup> Higher rates of corneal collagen remodeling were observed in pediatric corneas when compared to adults leading to more rapid ectasia progression.<sup>42</sup> For these reasons, we choose 4-week-old mice which are not adult yet.

Some patients develop complications of wound-healing related to the formation of stromal haze with reduced corneal transparency after PRK, or related to failure with possible ectasia after laser in situ keratomileusis.<sup>43</sup> The mouse model developed in our study tends to mimic this kind of stromal haze. Stromal haze was obtained 3 weeks after N<sub>2</sub> application as evidenced by slit-lamp observation (Figure 1C). Both



corneal backscattering scores determined by OCT and slit-lamp opacity were significantly increased in N<sub>2</sub>-injured eyes compared with those in contralateral control eyes, showing the loss of corneal transparency after N<sub>2</sub> application.

The corneal wound-healing cascade in response to the N<sub>2</sub> injury was initiated by an inflammatory response. IVCM and flow cytometry analysis showed the presence of inflammatory cells in the cornea just after N<sub>2</sub> application (Figure 4). This inflammatory phenotype was correlated with an overexpression of the CD11b marker in the cornea a few hours after N<sub>2</sub> injury. O'Brien et al demonstrated that the inflammatory response associated with the corneal-healing process after excimer laser PRK is characterized predominantly by macrophage infiltration.<sup>44</sup> In addition, macrophages can secrete elastase and collagenase and ingest dead tissue or degenerated cells that are important for tissue repair and reorganization.<sup>45,46</sup>

A series of phenotypic changes were induced at the same time or few hours after the inflammatory response such as apoptosis of a subpopulation of keratocytes at the site of injury evidenced with IVCM (Figure 1K) and TUNEL assay (Figure 1P). This finding was also demonstrated following the epithelial scrapping of mouse cornea<sup>47</sup> and after PRK which includes trauma to the corneal epithelium.<sup>48</sup> Studies have suggested that this regulated cell death is mediated by cytokines released from the injured epithelium such as interleukin-1 (IL-1) and tumor necrosis factor-alpha (TNF $\alpha$ ).<sup>47,49</sup>

Furthermore, our results showed the presence of myofibroblasts visualized with IVCM (Figure 1I) and revealed by  $\alpha$ -SMA staining (Figure 1M). These observations were in agreement with previous studies showing the process of repair in the corneal stroma characterized by keratocyte cell death followed by further transition of a subpopulation of remaining keratocytes to a repair or activated phenotype.<sup>50</sup> Myofibroblasts, first identified in skin wounds,<sup>51</sup> are thought to be responsible for wound contraction as well as ECM deposition and organization during corneal repair. Torricelli et al described that myofibroblasts and the disorganized ECM produced by these cells are critical determinants of the level and persistence of stromal opacity after corneal injury.<sup>52</sup> The presence of collagen type III staining after N<sub>2</sub> application (Figure 2J) was associated with the development of these cells. Accumulation of collagen type III, which is not normally present in the corneal stroma, alters the organization of the collagen lamellae resulting in augmented stromal opacity. The same observation was made by Shojaati et al in the development of their mouse model of corneal opacity. In their study, corneal epithelial debridement and removal of the basement membrane were obtained by passing an AlgerBrush over the central 2 mm of the mouse cornea. They demonstrated synthesis of collagen type III, development of fibrotic scar tissue, and loss of corneal transparency.<sup>53</sup> Three weeks after N<sub>2</sub> injury, a full-thickness epithelium was renewed featuring enhanced epithelial cell proliferation demonstrated by EdU staining (Figure S2N; Movies S2) and increased epithelial thickness (Figure S2U). Our mouse model also included disruption of the epithelial basement membrane (Figure S2P,R,T) which was likely to be a key effect in the loss of corneal transparency.<sup>53</sup> In a mouse model of penetrating keratoplasty, a disturbance to the basement membrane was

shown to be associated with transforming growth factor-beta (TGF- $\beta$ ) release by corneal epithelial cells inducing the transformation of keratocytes into myofibroblasts.<sup>54</sup> It is hypothesized that defective regeneration of the basement membrane allows key profibrotic growth factors, including TGF- $\beta$ 1 and TGF- $\beta$ 2, to penetrate the stroma at sustained levels necessary to drive the development and maintenance of fibrosis.<sup>55</sup>

Our study showed that corneal rigidity measured by OCT-SWE was significantly increased after N<sub>2</sub> injury (Figure 4D). This is in accordance with what was described in the literature by Raghunathan and his group. In their study, the atomic force microscopy-determined elastic modulus of rabbit cornea was increased after epithelial debridement and phototherapeutic keratectomy compared with presurgical values. This change coincides initially with the development of edema, inflammation, presence of myofibroblasts, and later with formation of stromal haze.<sup>56</sup> A low ocular rigidity was described in patients with myopia<sup>57</sup> or keratoconus. These findings show that corneal biomechanics depend on the condition of the cornea. In our study, increased corneal rigidity was associated with scar formation and changes in stromal striae morphology. Stromal striae are associated with the biomechanical behavior of cornea, that is, corneal viscoelasticity.<sup>58</sup> After N<sub>2</sub> application, stromal striae looked hyporeflexive and surrounded by hyperreflexive ECM, resembling what is observed in bullous keratopathy.<sup>58</sup> Whether increased rigidity results from both scarring and changes in stromal striae or only from scarring with striae changes resulting from the ECM changes cannot yet be determined. Corneal fibrosis in our mouse model was associated with impaired vision, as shown by the OTR analysis demonstrating a significant decrease in visual acuity in the N<sub>2</sub>-injured eye (Figure 4E,F).

## 4.2 | Therapeutic effect of SSCs

The characterization of multipotent stem cells in the human corneal stroma<sup>15,16,20</sup> has opened up the possibility of developing new therapeutic approaches for treating corneal stromal disorders. We used an original technique to grow SSC from limbal explants including scrapping of the limbal epithelium, enzymatic digestion of the explants, and culture with E8 medium supplemented with TGF- $\beta$ 1 and FGF-2 with no EGF. Scrapping off the epithelial cells is known to cause keratocytes apoptosis in vivo through release of IL-1 by injured epithelial cells.<sup>59</sup> We were able to ex vivo culture alive cells in this way probably because limbal explants were enzymatically digested just after epithelial scrapping. In our study, SSCs were injected after corneal opacity development in mice. We showed that injected MSSCs prelabeled with DiO or EdU were found in the N<sub>2</sub>-injured cornea 1 month after injection and had migrated within the corneal stroma (Figure 5B; Figure S3B). No inflammation or rejection was observed in response to these cells. The same finding was observed by Basu et al, after transplantation of SSC embedded in fibrin gel in mouse cornea after corneal epithelial debridement.<sup>25</sup> These cells probably secrete immunomodulatory molecules that exert beneficial effects on inflammation. Hertsberg et al suggest that SSCs prevent deposition of fibrotic

tissue by their secretion of TNF-inducible gene 6, a protein known to regulate neutrophil migration.<sup>17</sup>

Injected MSSC demonstrated the ability to grow and had a paracrine effect on adjacent epithelial cells (Figure 5N). Epithelial and keratocyte cell growth resulted in the reduction of corneal stromal haze revealed by decreases in both slit-lamp opacity score (Figure 7B) and corneal backscattering (Figure 7C). No significant difference between sham and MSSC injection was observed for slit-lamp opacity score and corneal backscattering (Figure 7B,C); first, we supposed that the sample size was not higher and the results will probably change if we enlarge the sample size. Second, the sham used here was DMEM/F-12, and we can hypothesize that this medium can improve the growth of stromal cells. In Figure 6L, stromal cell density in sham-injected cornea was higher with no significance than in N<sub>2</sub>-injured cornea demonstrating an induction of stromal cell growth after sham injection. DMEM/F-12 is a widely used basal medium for supporting the growth of many different mammalian cells including glial cells, fibroblasts, human endothelial cells, and rat fibroblasts. Absence of collagen type III, restoration of normal stromal lamellae, and reduction in fibril diameter in MSSC-injected cornea demonstrated the ability of MSSC to promote regeneration of native stromal tissue during wound repair. Basu et al observed that in their corneal epithelial debridement mouse model, limbal biopsy-derived stromal cells induce deposition of a native stromal tissue rather than scar tissue in healing wounds.<sup>25</sup> Recent studies showed that SSC differentiate into keratocytes and secrete collagens *in vitro*<sup>16,20-22</sup> and *in vivo*.<sup>18,25</sup>

Interestingly, prelabeled HSSC showed different fate compared with MSSC. In fact, the former were still detected 3 months after intrastromal injection whereas the latter were no longer detected following the first month. As labeling is lost with cell divisions, we can hypothesize that xenogeneic HSSC divide slower than allogeneic MSSC after intrastromal injection.

Corneal rigidity measured 3 months after MSSC injection was lower than that measured after sham injection (Figure S5A). Given the low number of animals (four for sham and three for MSSC injection) used for this experiment, no statistical comparison could be done. Decreased corneal rigidity associated with MSSC injection confirms the ability of MSSC to remodel corneal ECM. This decrease in corneal rigidity was associated with decreased stromal scarring and restoration of the normal appearance of stromal striae. This result was in accordance with the improvement of the visual acuity in our mouse model after SSC injection showed by the measurement of the optokinetic response (Figure S5B). However, the comparison of MSSC-injected with sham-injected eyes was not significant probably due to the low number of eyes which results in low statistical power.

In our model, the restoration of corneal transparency after SSC injection was associated with transition from the myofibroblast to the keratocyte phenotype of corneal stromal cells, decreased collagen III synthesis, improvement in the stromal lamellae structure/organization, paracrine effect of SSC on resident corneal epithelial cells, and regeneration of the corneal epithelial basement membrane. Mechanisms driving the interaction between injected MSSC and resident epithelial cells and restoration of corneal transparency need to be further studied to better understand the regenerative properties of SSC.

Furthermore, our study shows that sham injection in N<sub>2</sub>-injured cornea was associated with increased stromal cell density and a trend, although nonsignificant, to improvement in corneal transparency. DMEM/F-12 medium was used for sham injection. This medium permits keratocyte growth *in vitro* and it may induce the same effect *in vivo*. The impact of two vehicles, 0.85% NaCl and water, both alone and supplemented with 1 mg/mL ascorbic acid, has been demonstrated previously in a well-established tree shrew model of myopia.<sup>60</sup>

In conclusion, our study demonstrated the ability of corneal SSCs to promote regeneration of transparent stromal tissue. Injection of corneal SSCs can constitute an alternative approach in the treatment of corneal scarring.

## ACKNOWLEDGMENTS

We are grateful to J. Dégardin, M. Simonutti, Q. César, and the staff of the Animal and Phenotyping facilities for help. We thank S. Fouquet from the Imaging facility, L. Riancho from the FACS facility, and K. Kessal for help, D. Godefroy and M. Belle for clearing and imaging procedures. We thank A. Planul for help on the graphical abstract. We thank Alexis Canette (Electron Microscopy Facility, Sorbonne Université, Institut de Biologie Paris-Seine FR3631) for electron microscopy analysis. This work was supported by grants from the "Fondation pour la Recherche Médicale" No.: DCM20121225759 and a European Research Council SYNERGY Grant scheme (HELMHOLTZ, ERC Grant Agreement # 610110)

## CONFLICT OF INTEREST

A. C. declared research funding from Dompé and Densmore. V. B. declared employment/leadership position with CHNO des 15-20 and consulting role with Chiesi (Parma, Italy). The other authors declared no potential conflicts of interest.

## AUTHOR CONTRIBUTIONS

D.G.: conception, design, execution, and analysis/interpretation of all experiments and writing of the manuscript; M.B.: IVCN, slit-lamp, and OCT examination, analysis of results, and revision of manuscript; K.G.: FFOCM, OCT-SWE examination, analysis of results, and revision of the manuscript; R.M.: IVCN, slit-lamp, and OCT examination; R.B., T.-M.N.: OCT-SWE examination; P.C.: inflammatory cell examination; A.C.: manuscript revision; V.-M.B.: conception, design, and interpretation of experiments, manuscript writing, and financial support.

## DATA AVAILABILITY STATEMENT

The data that support the findings of this study are available within the manuscript and supplementary material.

## ORCID

Djida Ghoubay  <https://orcid.org/0000-0002-2282-5172>

Vincent M. Borderie  <https://orcid.org/0000-0002-1395-8483>

## REFERENCES

1. Davies SB, Di Girolamo N. Corneal stem cells and their origins: significance in developmental biology. *Stem Cells Dev.* 2010;19:1651-1662.

2. Hassell JR, Birk DE. The molecular basis of corneal transparency. *Exp Eye Res.* 2010;91:326-335.
3. Waring GO, Bourne WM, Edelhauser HF, et al. The corneal endothelium. Normal and pathologic structure and function. *Ophthalmology.* 1982;89:531-590.
4. Zhang J, Sisley AMG, Anderson AJ, et al. Characterization of a novel collagen scaffold for corneal tissue engineering. *Tissue Eng Part C Methods.* 2015;22:165-172.
5. Lwigale PY, Cressy PA, Bronner-Fraser M. Corneal keratocytes retain neural crest progenitor cell properties. *Dev Biol.* 2005;288:284-293.
6. Creuzet S, Couly G, Le Douarin NM. Patterning the neural crest derivatives during development of the vertebrate head: insights from avian studies. *J Anat.* 2005;207:447-459.
7. Gage PJ, Rhoades W, Prucka SK, Hjalt T. Fate maps of neural crest and mesoderm in the mammalian eye. *Invest Ophthalmol Vis Sci.* 2005;46:4200-4208.
8. Yoshida S, Shimmura S, Shimazaki J, Shinozaki N, Tsubota K. Serum-free spheroid culture of mouse corneal keratocytes. *Invest Ophthalmol Vis Sci.* 2005;46:1653-1658.
9. West-Mays JA, Dwivedi DJ. The keratocyte: corneal stromal cell with variable repair phenotypes. *Int J Biochem Cell Biol.* 2006;38:1625-1631.
10. Hay ED. Development of the vertebrate cornea. *Int Rev Cytol.* 1980;63:263-322.
11. Calloni GW, Glavieux-Pardanaud C, Le Douarin NM, et al. Sonic hedgehog promotes the development of multipotent neural crest progenitors endowed with both mesenchymal and neural potentials. *Proc Natl Acad Sci USA.* 2007;104:19879-19884.
12. Calloni GW, Le Douarin NM, Dupin E. High frequency of cephalic neural crest cells shows coexistence of neurogenic, melanogenic, and osteogenic differentiation capacities. *Proc Natl Acad Sci USA.* 2009;106:8947-8952.
13. Wilson SE, Netto M, Ambrósio R. Corneal cells: chatty in development, homeostasis, wound healing, and disease. *Am J Ophthalmol.* 2003;136:530-536.
14. Fini ME, Stramer BM. How the cornea heals: cornea-specific repair mechanisms affecting surgical outcomes. *Cornea.* 2005;24:S2-S11.
15. Du Y, Funderburgh ML, Mann MM, et al. Multipotent stem cells in human corneal stroma. *STEM CELLS.* 2005;23:1266-1275.
16. Ghoubay-Benallaoua D, de Sousa C, Martos R, et al. Easy xeno-free and feeder-free method for isolating and growing limbal stromal and epithelial stem cells of the human cornea. *PLoS One.* 2017;12:e0188398.
17. Hertszenberg AJ, Shojaati G, Funderburgh ML, Mann MM, du Y, Funderburgh JL. Corneal stromal stem cells reduce corneal scarring by mediating neutrophil infiltration after wounding. *PLoS One.* 2017;12:e0171712.
18. Du Y, Carlson EC, Funderburgh ML, et al. Stem cell therapy restores transparency to defective murine corneas. *STEM CELLS.* 2009;27:1635-1642.
19. Wu J, Du Y, Mann MM, et al. Corneal stromal stem cells versus corneal fibroblasts in generating structurally appropriate corneal stromal tissue. *Exp Eye Res.* 2014;120:71-81.
20. Du Y, Sundarraj N, Funderburgh ML, et al. Secretion and organization of a cornea-like tissue in vitro by stem cells from human corneal stroma. *Invest Ophthalmol Vis Sci.* 2007;48:5038-5045.
21. Wu J, Du Y, Mann MM, et al. Bioengineering organized, multilamellar human corneal stromal tissue by growth factor supplementation on highly aligned synthetic substrates. *Tissue Eng Part A.* 2013;19:2063-2075.
22. Wu J, Du Y, Watkins SC, et al. The engineering of organized human corneal tissue through the spatial guidance of corneal stromal stem cells. *Biomaterials.* 2012;33:1343-1352.
23. Syed-Picard FN, Du Y, Hertszenberg AJ, et al. Scaffold-free tissue engineering of functional corneal stromal tissue. *J Tissue Eng Regen Med.* 2018;12:59-69.
24. Funderburgh JL, Funderburgh ML, Du Y. Stem cells in the limbal stroma. *Ocul Surf.* 2016;14:113-120.
25. Basu S, Hertszenberg AJ, Funderburgh ML, et al. Human limbal biopsy-derived stromal stem cells prevent corneal scarring. *Sci Transl Med.* 2014;6:266ra172.
26. Erie JC. Corneal wound healing after photorefractive keratectomy: a 3-year confocal microscopy study. *Trans Am Ophthalmol Soc.* 2003;101:293-333.
27. Hollingsworth JG, Efron N, Tullo AB. In vivo corneal confocal microscopy in keratoconus. *Ophthalmic Physiol Opt.* 2005;25:254-260.
28. Borderie M, Grieve K, Irsch K, et al. New parameters in assessment of human donor corneal stroma. *Acta Ophthalmol.* 2017;95:e297-e306.
29. Nguyen T-M, Arnal B, Song S, Huang Z, Wang RK, O'Donnell M. Shear wave elastography using amplitude-modulated acoustic radiation force and phase-sensitive optical coherence tomography. *J Biomed Opt.* 2015;20:016001.
30. Dubois A, Grieve K, Moneron G, Lecaque R, Vabre L, Boccard C. Ultrahigh-resolution full-field optical coherence tomography. *Appl Optics.* 2004;43:2874-2883.
31. Grieve K, Paques M, Dubois A, Sahel J', Boccard C, le Gargasson JF. Ocular tissue imaging using ultrahigh-resolution, full-field optical coherence tomography. *Invest Ophthalmol Vis Sci.* 2004;45:4126-4131.
32. Ghoulai W, Grieve K, Bellefqih S, et al. Full-field optical coherence tomography of human donor and pathological corneas. *Curr Eye Res.* 2015;40:526-534.
33. Belle M, Godefroy D, Dominici C, et al. A simple method for 3D analysis of immunolabeled axonal tracts in a transparent nervous system. *Cell Rep.* 2014;9:1191-1201.
34. Ghoubay-Benallaoua D, Basli E, Goldschmidt P, et al. Human epithelial cell cultures from superficial limbal explants. *Mol Vis.* 2011;17:341-354.
35. Reichman S, Slembrouck A, Gagliardi G, et al. Generation of storable retinal organoids and retinal pigmented epithelium from adherent human iPSC cells in xeno-free and feeder-free conditions. *STEM CELLS.* 2017;35:1176-1188.
36. Uchida S, Yokoo S, Yanagi Y, et al. Sphere formation and expression of neural proteins by human corneal stromal cells in vitro. *Invest Ophthalmol Vis Sci.* 2005;46:1620-1625.
37. Grieve K, Georgeon C, Andreiuolo F, et al. Imaging microscopic features of keratoconic corneal morphology. *Cornea.* 2016;35:1621-1630.
38. Rabinowitz YS. Keratoconus. *Surv Ophthalmol.* 1998;42:297-319.
39. El Rami H, Chelala E, Dirani A, et al. An update on the safety and efficacy of corneal collagen cross-linking in pediatric keratoconus. *Biomed Res Int.* 2015;2015:257927.
40. Raiskup-Wolf F, Hoyer A, Spoerl E, Pillunat LE. Collagen crosslinking with riboflavin and ultraviolet-a light in keratoconus: long-term results. *J Cataract Refract Surg.* 2008;34:796-801.
41. Mukhtar S, Ambati BK. Pediatric keratoconus: a review of the literature. *Int Ophthalmol.* 2018;38:2257-2266.
42. Rehany U, Rumelt S. Corneal hydrops associated with vernal conjunctivitis as a presenting sign of keratoconus in children. *Ophthalmology.* 1995;102:2046-2049.
43. Ljubimov AV, Saghizadeh M. Progress in corneal wound healing. *Prog Retin Eye Res.* 2015;49:17-45.
44. O'Brien TP, Li Q, Ashraf MF, et al. Inflammatory response in the early stages of wound healing after excimer laser keratectomy. *Arch Ophthalmol (Chicago, Ill 1960).* 1998;116:1470-1474.
45. Nathan CF. Secretory products of macrophages. *J Clin Invest.* 1987;79:319-326.
46. Werb Z, Gordon S. Secretion of a specific collagenase by stimulated macrophages. *J Exp Med.* 1975;142:346-360.
47. Wilson SE, He Y-G, Weng J, et al. Epithelial injury induces keratocyte apoptosis: hypothesized role for the interleukin-1 system in the modulation of corneal tissue organization and wound healing. *Exp Eye Res.* 1996;62:325-338.

48. Helena MC, Baerveldt F, Kim WJ, Wilson SE. Keratocyte apoptosis after corneal surgery. *Invest Ophthalmol Vis Sci.* 1998;39:276-283.
49. MOHAN RR, LIANG Q, W-J KIM, et al. Apoptosis in the cornea: further characterization of Fas/Fas ligand system. *Exp Eye Res.* 1997;65:575-589.
50. Jester JV, Rodrigues MM, Herman IM. Characterization of avascular corneal wound healing fibroblasts. New insights into the myofibroblast. *Am J Pathol.* 1987;127:140-148.
51. Jester JV, Petroll WM, Cavanagh HD. Corneal stromal wound healing in refractive surgery: the role of myofibroblasts. *Prog Retin Eye Res.* 1999;18:311-356.
52. Torricelli AAM, Wilson SE. Cellular and extracellular matrix modulation of corneal stromal opacity. *Exp Eye Res.* 2014;129:151-160.
53. Shojaati G, Khandaker I, Sylakowski K, Funderburgh ML, du Y, Funderburgh JL. Compressed collagen enhances stem cell therapy for corneal scarring. *STEM CELLS TRANSLATIONAL MEDICINE.* 2018;7:487-494.
54. Stramer BM, Zieske JD, Jung J-C, Austin JS, Fini ME. Molecular mechanisms controlling the fibrotic repair phenotype in cornea: implications for surgical outcomes. *Invest Ophthalmol Vis Sci.* 2003;44:4237-4246.
55. Medeiros CS, Marino GK, Santhiago MR, Wilson SE. The corneal basement membranes and stromal fibrosis. *Invest Ophthalmol Vis Sci.* 2018;59:4044-4053.
56. Raghunathan VK, Thomasy SM, Strøm P, et al. Tissue and cellular biomechanics during corneal wound injury and repair. *Acta Biomater.* 2017;58:291-301.
57. Chansangpetch S, Panpruk R, Manassakorn A, et al. Impact of myopia on corneal biomechanics in glaucoma and nonglaucoma patients. *Invest Ophthalmol Vis Sci.* 2017;58:4990-4996.
58. Grieve K, Ghoubay D, Georgeon C, et al. Stromal striae: a new insight into corneal physiology and mechanics. *Sci Rep.* 2017;7:13584.
59. Wilson SE, Liu JJ, Mohan RR. Stromal-epithelial interactions in the cornea. *Prog Retin Eye Res.* 1999;18:293-309.
60. Ward AH, Siegwart JT, Frost MR, et al. The effect of intravitreal injection of vehicle solutions on form deprivation myopia in tree shrews. *Exp Eye Res.* 2016;145:289-296.

## SUPPORTING INFORMATION

Additional supporting information may be found online in the Supporting Information section at the end of this article.

**How to cite this article:** Ghoubay D, Borderie M, Grieve K, et al. Corneal stromal stem cells restore transparency after N<sub>2</sub> injury in mice. *STEM CELLS Transl Med.* 2020;1-19. <https://doi.org/10.1002/sctm.19-0306>